REVIEW

Check for updates

Structural design and preparation of Ti₃C₂Tx MXene/polymer composites for absorption-dominated electromagnetic interference shielding

Qimei Zhang, [ID] ab Qi Wang,a Jian Cui,a Shuai Zhao, [ID] a Guangfa Zhang, [ID] a Ailin Gaoa and Yehai Yan [ID] *a

Electromagnetic interference (EMI) is a pervasive and harmful phenomenon in modern society that affects the functionality and reliability of electronic devices and poses a threat to human health. To address this issue, EMI-shielding materials with high absorption performance have attracted considerable attention. Among various candidates, two-dimensional MXenes are promising materials for EMI shielding due to their high conductivity and tunable surface chemistry. Moreover, by incorporating magnetic and conductive fillers into MXene/polymer composites, the EMI shielding performance can be further improved through structural design and impedance matching. Herein, we provide a comprehensive review of the recent progress in MXene/polymer composites for absorption-dominated EMI shielding applications. We summarize the fabrication methods and EMI shielding mechanisms of different composite structures, such as homogeneous, multilayer, segregated, porous, and hybrid structures. We also analyze the advantages and disadvantages of these structures in terms of EMI shielding effectiveness and the absorption ratio. Furthermore, we discuss the roles of magnetic and conductive fillers in modulating the electrical properties and EMI shielding performance of the composites. We also introduce the methods for evaluating the EMI shielding performance of the materials and emphasize the electromagnetic parameters and challenges. Finally, we provide insights and suggestions for the future development of MXene/polymer composites for EMI shielding applications.

aKey Lab of Rubber-Plastics, Ministry of Education, Shandong Provincial Key Lab of Rubber-Plastics, School of Polymer Science and Engineering, Qingdao University of Science and Technology, Qingdao, 266042, China. E-mail: yhyan@qust.edu.cn

bSchool of Materials and Environmental Engineering, Chizhou University, Chizhou, 247000, China. E-mail: zhangqm@czu.edu.cn

Qimei Zhang received her bachelor's degree from Qingdao University of Science and Technology in 2006 and her master's degree from Zhejiang Sci-Tech University in 2009. She then worked at Chizhou University. She is currently pursuing her PhD at Qingdao University of Science and Technology under the supervision of Professor Yehai Yan. Her research work focuses on electromagnetic shielding polymer composite materials.

Professor Yehai Yan obtained his PhD degree in polymer physics and chemistry from the Institute of Chemistry at the Chinese Academy of Sciences in 2002. He then worked as a research fellow at Nanyang Technological University of Singapore (2002–2006) and as a Humboldt fellow at Leibniz-Institut für Polymerforschung Dresden of Germany (2008–2009). Currently, he is a full professor in the School of Polymer Science and Engineering at Qingdao University of Science and Technology. His research interests include high-performance polymer composites and polymer membranes.

Introduction

Portable devices and communication technologies are ubiquitous in today's society. However, many of these technologies are susceptible to interference from high-frequency electromagnetic (EM) radiation. EM interference (EMI) adversely affects human health, information security, and precision equipment.[1,2] Therefore, efficient EMI-shielding materials are urgently required.[3] The development of lightweight and high-performance absorption-dominated green EMI-shielding materials has received significant attention. There have been remarkable advances in the structural design of MXene/polymer composites for absorption-dominated green EMI shielding applications.[3]

To realize outstanding shielding performance, EMI-shielding materials should have high reflection and absorption losses based on Schelkunoff's EM wave (EMW) interfacial conduction theory.[4] Homogeneous,[5] layered,[6] porous,[7] segregated,[8–10] and hybrid composites with conductive networks are efficient for EMI shielding because incident EMWs are dissipated by multiple internal reflections and dielectric losses (*e.g.*, conduction, interfacial polarization, and dipole polarization losses) within the material.

Magnetic/conductive composites with complete conductive and magnetic networks also exhibit favorable EMI shielding[11] based on dielectric and magnetic losses.[12] Specifically, the conductive network is responsible for dielectric losses due to charge transfer and polarization effects,[13,14] while the magnetic network is responsible for magnetic losses due to magnetic resonance, coupling, and eddy currents. Additionally, the magnetic network can enhance the dielectric losses by increasing the internal reflection and interfacial dissipation of EMWs.[15]

To achieve high EMI absorption shielding performance, the concept of magnetic filler and MXene separation was introduced in the design of magnetic/MXene/polymer composites based on the significant differences in conductivity between the magnetic filler and MXene.[16] In addition, when the impedance of the shielding material is well matched with that of the free space, EMWs are more likely to penetrate the shielding material and be absorbed.[17] Impedance matching is crucial for achieving green EMI shielding that relies on absorption.[18]

In this review, the structural design and EMI-shielding mechanisms of homogeneous, multilayer, porous, segregated, hybrid, and conductive/magnetic MXene/polymer composites are introduced (Fig. 1), with a particular focus on $Ti_3C_2T_x$/polymer composites. The electromagnetic parameters, impedance matching, research progress, and absorption properties of EMI-shielding materials are discussed.

Absorption EMI shielding requires not only ideal impedance matching but also efficient EMW attenuation, which can effectively reduce the reflection and transmission of EMWs. In this review, we emphasize the necessity of the integrity and continuity of the conductive network in MXene/polymer composites by separating the conductive filler from the polymer matrix. We also suggest ways to improve magnetic losses
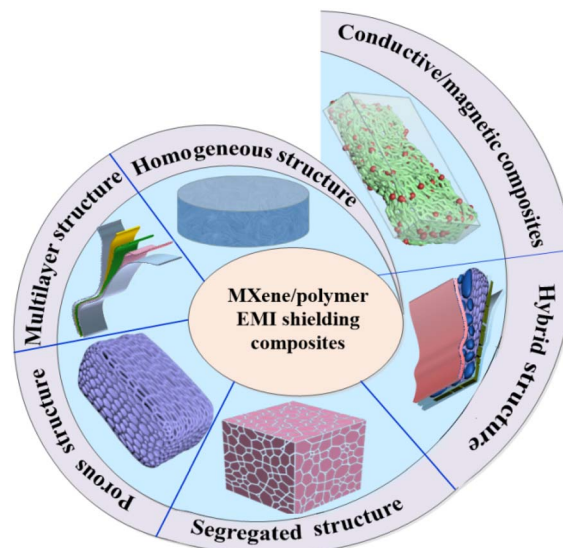

Fig. 1 Structural design of MXene/polymer EMI-shielding composites.

and achieve excellent impedance matching by designing magnetic/conducting composite materials. The synergistic effect of dielectric and magnetic losses contributes to efficient and green absorption EMI shielding. Finally, the direction of future research on MXene/polymer composites for EMI shielding is discussed.

Methods of evaluating EMI-shielding performance

The effectiveness of materials in preventing the transmission of incident EMWs is measured based on a concept known as EMI-shielding effectiveness (EMI SE).[19,20] The EMI SE represents the difference between the incident and transmitted EM power as a decibel logarithm.[21,22] For commercial applications, an EMI SE of above 20 dB (*i.e.*, an EMW attenuation effectiveness of at least 99%) is required; for military applications, this increases to 60 dB.[23,24]

EMI-shielding mechanisms

EMI-shielding mechanisms are assessed using eddy current effects, EM field theory, and transmission line theory. Transmission line theory[25] is widely used because of its convenient calculation and high accuracy for materials with uniform or dense structures. According to Schelkunoff's transmission line theory, the total EMI SE (SE_T; eqn (1)) of a material constitutes the shielding effectiveness by reflection losses (SE_R), absorption losses (SE_A), and multiple reflection losses (SE_M) (eqn (2)–(4), respectively).[26]

$$SE_T = SE_A + SE_R + SE_M \quad (1)$$

$$SE_R = 168.2 - 10\log(f\mu_r/\sigma_r) \quad (2)$$

$$SE_A = 131.43t(f\mu_r\sigma_r)^{1/2} \quad (3)$$

$$SE_M = 20 \log(1 - e^{-2t/\delta}) \tag{4}$$

where f is the EMW frequency, μ_r is the relative magnetic permeability, σ_r is the electrical conductivity relative to pure copper, and t is the thickness of the shielding material. Eqn (2)–(4) are applicable when $t > \delta$, where skin depth δ is the depth at which the energy of the incident EMW decreases to $1/e$:[27–31]

$$\delta = \frac{1}{\sqrt{f \mu \pi \sigma}} \tag{5}$$

Here, $\mu = \mu_0 \mu_r$, where μ_0 is the magnetic permeability of vacuum $(4\pi \times 10^{-7} \text{ H m}^{-1})$.[32] The phenomenon of EMW energy attenuation with the thickness of a conductive composite is known as the skin effect.[33] This effect is due to coupling between the displacement currents of EMWs that strike the surface of a conductive composite and those of the composite itself, creating a perpendicular magnetic field that induces a back electromotive force that opposes the EMWs. The deeper the EMWs penetrate the composite, the more they are attenuated by the skin effect.

In EMI-shielding materials, both absorption losses (SE_A) and reflection losses (SE_R) increase as the relative electrical conductivity increases, resulting in an increase in total SE (SE_T). In addition, EMW attenuation increases with increasing thickness. Attenuation of the EMW energy increases in composites with a certain EMW frequency and thickness. On the other hand, as the relative magnetic permeability increases, SE_A increases and SE_R decreases. This causes SE_T to first decrease and then increase,[34] while the EMI-shielding mechanism transitions to an absorption-dominated mechanism.[35] For most practical applications, absorption-dominated EMI shielding is preferred because EMW reflection causes secondary EM pollution.

Multiple reflection losses (SE_M) are mostly related to the thickness and skin depth of the shielding material. In high-frequency electric fields, the contribution of SE_M approaches zero[36] and can be disregarded when the skin depth is considerably less than the shield thickness, or for homogeneous materials with a SE_T of more than 15 dB.[37] However, in materials with numerous heterogeneous interfaces or pores, incident EMWs lose significant energy due to multiple reflections owing to the interfacial impedance mismatch, particularly if the material thickness is less than the skin depth. Thus, the significance of multiple reflection losses cannot be disregarded when determining a heterogeneous material's ability to absorb EMWs.[37,38]

Conductive MXene/polymer composites contain numerous heterogeneous interfaces, causing incident EMWs to be entirely dissipated owing to dielectric losses (multiple heterogeneous interfacial polarization, dipole polarization, and conduction losses). If the composite contains a magnetic filler, magnetic losses (magnetic resonance, magnetic coupling, and eddy current losses) also apply. Under the synergistic effect of dielectric and magnetic losses, magnetic/conductive MXene/polymer composites exhibit high-performance absorption-dominated EMI shielding.[12]

Calculation of EMI SE

EMI SE can be measured using various techniques, including flanged coaxial devices,[39] shielded room window tests, double shielded box tests, and gigahertz transverse EM cell tests.[40] A vector network analyzer[41] is employed during lab testing to determine the scattering parameter (S-parameter) and compute EMI SE using eqn (6)–(11).[42]

$$R = P_r/P_i = |S_{11}|^2 = |S_{22}|^2 \tag{6}$$

$$T = P_t/P_i = |S_{12}|^2 = |S_{21}|^2 \tag{7}$$

$$A + R + T = 1 \tag{8}$$

where R, A, and T are the reflection, absorption, and transmission power coefficients, respectively; P, P_r, and P_t are the incident, reflected, and transmitted powers of the EMWs, respectively; S_{12} and S_{21} represent the forward and inverse transmission coefficients, respectively; and S_{11} and S_{22} represent the reflection coefficients from ports 1 and 2, respectively. The formulas for EMI SE are as follows:[11]

$$SE_R = -10 \log(1 - R) = 10 \log(1/(1 - |S_{11}|^2)) \tag{9}$$

$$SE_A = 10 \log((1 - R)/T) = 10 \log((1 - |S_{11}|^2)/|S_{21}|^2) \tag{10}$$

$$SE_T = SE_A + SE_R + SE_M \approx SE_A + SE_R = 10 \log|S_{21}|^2 \tag{11}$$

Overview of MXene/polymer composites

A conductive composite with excellent electrical conductivity can be obtained by mixing a conductive filler and an insulating polymer matrix, provided that the filler forms a percolating network for charge carrier transport throughout the composite. These composites are cost-effective and easy to fabricate, and various types have been developed for EMI shielding applications.[43] Studies on improving the EMI-shielding performance of polymer composites typically focus on optimizing the conductive filler and structural design. Conductive fillers include two-dimensional (2D) transition metal carbides/nitrides (MXene),[44] carbon-based materials (e.g., carbon black, graphite, reduced graphene oxide (rGO), and carbon nanotubes (CNTs));[39,45] metals (e.g., silver nanowires (AgNWs), copper,[46] and aluminum powder),[47] and magnetic materials (e.g., MXene/Ni nanocomposites, MXene@Fe_2O_3, and Fe_3O_4-grafted graphene).[48,49] Of these, MXenes are used extensively in EMI-shielding materials.

Overview of MXenes

MXenes are a prominent class of materials in the field of materials science. These 2D materials possess metallic conductivity and are derived from selectively removing atomic layers from a ternary layered MAX precursor, where M is an early type transition metal (Ti, Zr, V, or Mo), A is a principal group

element (Al or Si), and X is C or N.[50] More than 80 types of MAX compounds have been reported. Al-series MXenes are often formed by selectively etching Al layers from an Al-based MAX compound using a fluorine-based acid.[51,52] However, this leaves numerous F terminations or functional groups at the surface, which reduces the electrochemical properties of the material. Several promising preparation methods that avoid dangerous fluorinated compounds and harsh etching conditions have been proposed. A method based on Lewis acid molten salts has also been reported.[53] These methods enable the fabrication of fluorine-free MXenes, although the reaction conditions can be demanding.

Since their discovery,[51] MXenes' excellent physical and chemical properties have been investigated in relation to their size. $Ti_3C_2T_x$, the most widely used MXene, has an excellent conductivity of 5000–8000 S cm^{-1},[44] which has led to its wide use in electrochemical energy storage systems,[54] sensors,[55] EMI-shielding materials,[44] and wearable electronics.[56] In particular, the high specific surface area, excellent hydrophilicity,[57] rich set of tunable functional surface groups, and excellent electrical properties of $Ti_3C_2T_x$ make it an efficient conductive filler for EMI-shielding materials.[58] However, its electrical conductivity is degraded if the thin layers stack together,[59] which is difficult to precisely regulate in polymer composites owing to the weak

interfacial bonding between $Ti_3C_2T_x$ flakes. This results in a failure to maximize the synergy, coupling, and multifunctional response mechanisms between different components.[55,56] Using the electro-static accumulation approach, in which aqueous ammonia or ammonium bicarbonate is added to the MXene supernatants, Zhang et al.[60] used NH^{4+} to address the stacking issue of $Ti_3C_2T_x$ sheets. Even without a polymer matrix, MXenes are excellent EMI-shielding materials. Monolayer[61] and multilayer MXenes can be produced by solution-based self-assembly from colloids of MXenes with hydrophilic functional groups owing to their good dispersion in water.

Wan et al.[61] proposed a sequential densification strategy that synergistically eliminated the voids between MXene flakes while enhancing the interlayer electron transport. Small MXene flakes were first intercalated to fill the voids between large multilayer flakes, followed by interfacial bridging with calcium and borate ions to eliminate the remaining voids, including those between monolayer flakes. This strategy overcame the common problem of electron transport between MXene flakes being interrupted by insulating polymer bonding agents, thereby increasing the electrical conductivity.

Yun et al.[62] studied the relationship between electrical conductivity, EMI SE, and $Ti_3C_2T_x$ film thickness. A 24-layer (55 nm thick) film shielded 99% (20 dB) of EMWs (Fig. 2a), and

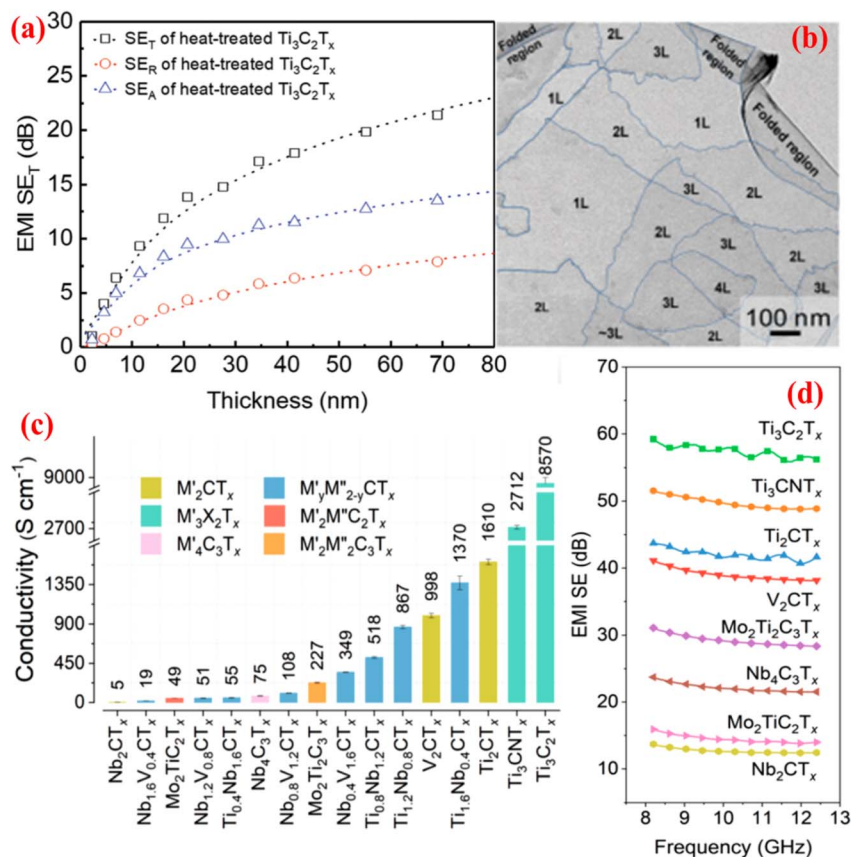Fig. 2 (a) EMI SE values of $Ti_3C_2T_x$ film after annealing at 400 °C and (b) transmission electron microscopy image of few-layer thick MXene film. Reproduced with permission from ref. 62 with permission from Wiley-VCH Verlag GmbH & Co. KGaA, Weinheim, © 2020. (c) Conductivity and (d) EMI SE of 5 μm-thick MXene films with different compositions. Reproduced from ref. 63 with permission from the American Chemical Society, © 2020.

a monolayer film shielded 20% of EMWs and transmitted 90% of the light (Fig. 2b). This is a testament to the outstanding EMI-shielding performance of $Ti_3C_2T_x$, and provides a theoretical basis for EMI-shielding $Ti_3C_2T_x$/polymer composites. Han et al.[63] studied 16 types of MXenes, including single-metal MXenes, ordered double-metal carbides, and MXenes with random solid solutes of M and X. Of these, $Ti_3C_2T_x$ had the best overall properties and conductivity (Fig. 2c). In addition, the EMI-shielding performance of these MXenes (in the form of 5 μm-thick films) was compared under X-band EMI (8.2–12.4 GHz), as shown in Fig. 2d. While several of the MXene films had EMI SEs of over 20 dB, $Ti_3C_2T_x$ achieved the highest average shielding performance of 55 dB. In another study, Shahzad et al.[37] prepared a 45 μm-thick $Ti_3C_2T_x$ film with an EMI SE of 92 dB, which inspired research[64] into multilayer MXenes as practical EMI-shielding materials.

MXene/polymer composites with novel structural assemblies can overcome issues with MXene stacking.[60] Moreover, they integrate the advantages of polymers and structural design, making them efficient EMI-shielding materials. Therefore, it is important to study MXene/polymer composite design strategies.[65]

Structural design of MXene/polymer composites

MXene/polymer composites have been fabricated with various architectures, such as homogeneous, multilayer, porous, segregated, and hybrid structures. The conductive filler can be optimized in terms of quantity, morphology, modification, and dispersion to enhance the conductance path and significantly increase conductivity. The incorporation of magnetic nano-fillers can further improve EMW absorption and reflection losses; thus, magnetic/conductive MXene/polymer composites exhibit excellent EMI-shielding performance.[66] The synergistic effect of conductive and magnetic fillers with suitable structural design can optimize the impedance matching and boost the EMI-shielding performance.[12] Therefore, these composites have excellent potential for commercialization. The EMI-shielding mechanisms of different kinds of MXene/polymer composites are discussed below.

EMI-shielding mechanisms of different MXene/polymer composite structures

Homogeneous MXene/polymer composites

Interfacial polarization and dielectric losses play major roles in dissipating EMWs in homogeneous MXene/polymer composites. The Maxwell–Wagner effect[49] states that charge carriers will accumulate at the interfaces of materials with different dielectric constants in mixed systems, resulting in interfacial polarization. Owing to the difference in conductivity between the polymer matrix and conductive filler (MXene), asymmetrically distributed charge carriers will accumulate at the MXene/polymer interfaces in homogeneous MXene/polymer composites, resulting in strong interfacial polarization and dielectric losses. Incident EMWs are also attenuated by the dielectric component and dissipated as heat through the composite.

Multilayer MXene/polymer composites

Multilayer structures substantially improve the EMI-shielding performance of MXene/polymer composites because they enhance the internal reflections of EMWs.[67] The shielding mechanism is shown in Fig. 3a. When incident EMWs (purple arrows) strike the composite surface, they are partially reflected (blue arrows) due to impedance mismatch at the air/composite interface.[68] The remaining EMWs travel to the first MXene layer, where some of their energy is absorbed or emitted in the form of thermal energy (red arrows), resulting in partial transmission of the EMWs (black arrows). Several mechanisms contribute to the attenuation of EMWs, including eddy current effects,[49] the local dipoles generated on the polar functional groups (–OH, –F, and –O) on the MXene surface under alternating EM fields,[37] and the local current in the MXene nanosheets due to ohmic loss. The EMW intensity is therefore substantially reduced each time it encounters an MXene layer. With multiple internal reflections and increased absorption losses, the energy of the transmitted wave decreases until it is completely attenuated or eliminated.[69]

Porous and segregated MXene/polymer composites

Porous and segregated MXene/polymer composites with conductive networks exhibit similar EMI-shielding behavior to multilayer structures, in that the high-frequency EMWs are attenuated by multiple reflection and absorption losses[51] and finally dissipate in the form of heat. When the loading of the conductive filler (MXene) exceeds the percolation threshold, an excellent conductive network is formed, resulting in impedance mismatch at the air/composite interface. However, unlike the discontinuous conductive networks in multilayer structures, porous and segregated structures contain a continuous three-dimensional (3D) or honeycomb-structured conductive network (Fig. 3b and c). The closed or partially closed cage structure in porous and segregated MXene/polymer composites facilitates EMW reflection and attenuation. EMWs that enter the material are dissipated due to repeated reflections at the heterogeneous interfaces and pores owing to impedance mismatch.[70] Thus, multiple reflection loss is the main EMI-shielding mechanism in porous and segregated MXene/polymer composites.

Owing to the large surface and interfacial areas of segregated nanocomposites, the EMI-shielding mechanism in these structures is much more complex than that in uniform conductive materials. The MXene network in segregated MXene/polymer nanocomposites encourages the incident EMWs to penetrate the composite rather than being reflected at the surface. Incident EMWs are effectively dissipated and attenuated at the surface and internal interfaces by multiple scattering and interfacial polarization losses, significantly increasing the absorption contribution. The charge carriers at the surfaces of the MXene sheets[37] interact with EMWs[69] and dissipate them by converting them to heat.

The capacitive structures that form between filler particles with different conductivities and between filler and matrix phases result in the accumulation, rearrangement, and inter-facial polarization of space charge in alternating electric fields.
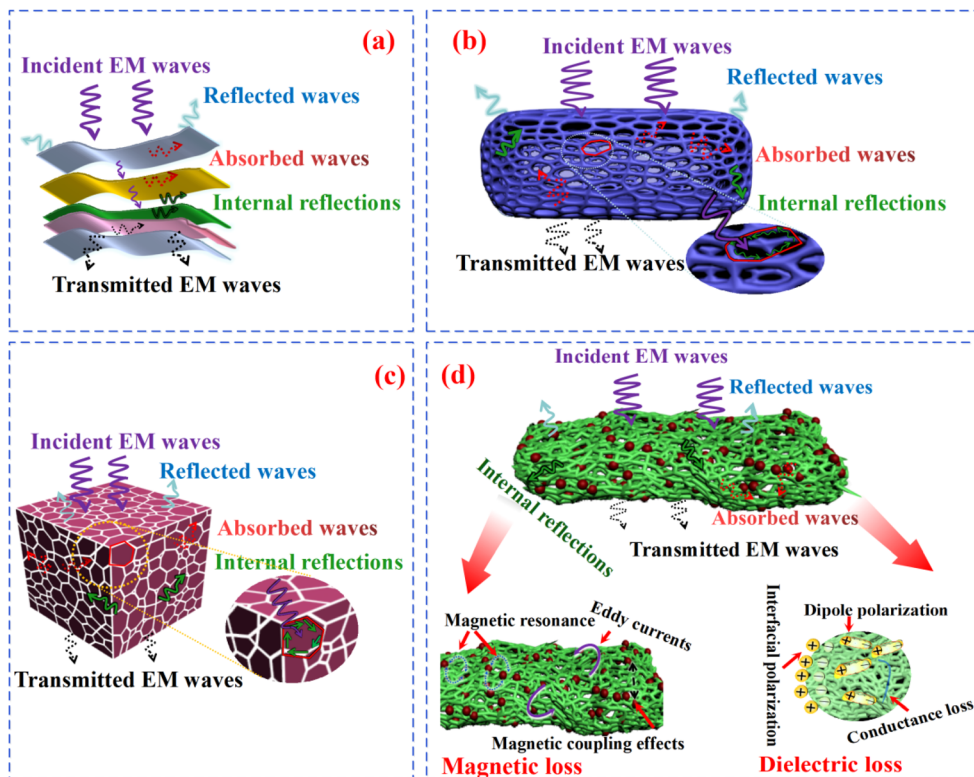
Fig. 3 EMI shielding mechanisms of different structures of MXene/polymer composites: (a) multilayer, (b) porous, (c) segregated, and (d) magnetic/conductive networks.

Honeycomb-structured conductive networks with rich interfaces exhibit large dipole polarization and dielectric losses. Similarly, 3D conductive networks further promote the transformation of EMWs to thermal energy.[71]

Hybrid MXene/polymer composites

Hybrid structures use a combination of homogeneous, multilayer, porous, and segregated structural features. Thus, multiple EMW absorption mechanisms occur, including dielectric losses, layer-by-layer dissipation, and cage-based EMW attenuation. Consequently, these materials have high EMI-shielding performance. However, the shielding mechanisms are far more complex than those in composites with a single structural feature.

Magnetic/conductive MXene/polymer composites

MXene/polymer composites with conductive and magnetic fillers exhibit outstanding EMI-shielding performance. The conductive network causes an EMW impedance mismatch at the composite/air interface, leading to reflection. The magnetic materials enhance the impedance matching at the conductive filler/air interface and increase EMW absorption. The shielding mechanism is shown in Fig. 3d. When incident EMWs strike the material, they are partially reflected from the highly conducting surface (blue arrows) owing to the numerous charge carriers. When the EMWs encounter $Ti_3C_2T_x$ flakes, they lose energy owing to dielectric losses (conduction, interfacial polarization,

and particle polarization losses) as well as multiple internal reflection losses. The magnetic filler (red particles) also consumes EMW energy through magnetic losses (magnetic response, magnetic coupling, and eddy current losses). When an EMW that has passed through a magnetic particle contacts a $Ti_3C_2T_x$ flake, owing to the differences in conductivity and refractive index between these phases, the impedance mismatch at their interface results in reflection of the EMW. Thus, composites with a large number of heterogeneous interfaces favor multiple reflection and absorption losses. Due to the synergistic effect between the conducting network and the magnetic filler, a large portion of EMWs can be consumed.

Progress of structural design in MXene/polymer composites

Homogeneous MXene/polymer composites

EMI-shielding composites with homogeneous structures usually comprise direct blends of conductive fillers in a polymer matrix. Increasing the conductive filler content up to the percolation threshold[72] facilitates the fabrication of a continuous conductive network, thus creating a path of conductance through the material and transforming it from insulator to conductor. Rajavel et al.[73] used solvent-assisted direct mixing and hot-pressing to prepare $Ti_3C_2T_x$/polyvinylidene fluoride (PVDF) nanocomposites (Fig. 4a), which had a good EMI SE of 48.47 dB at a thickness of 2 mm. The shielding mechanism of

homogeneous MXene/polymer composites is shown in Fig. 4b. Wang *et al.*[74] combined an epoxy and curing agent in acetone solution to create a $Ti_3C_2T_x$ suspension (Fig. 4c). The annealed $Ti_3C_2T_x$/epoxy nanocomposite with 15 wt% $Ti_3C_2T_x$ had an optimal electrical conductivity of 105 S m^{-1} and EMI SE of 41 dB.

Printing is another convenient method for producing homogeneous MXene/polymer composites. Vural *et al.*[5] printed MXene/protein electrodes on various substrates using an ink made of titanium carbide MXene nanosheets and squid ring teeth protein. The printed electrodes on polyethylene terephthalate substrates had an electrical conductivity of 1080 S cm^{-1} and an excellent EMI SE of 50 dB with a film thickness of 1.35 μm.

Direct ink writing 3D printing technology enables the fabrication of complex 3D structures from MXene nanosheets with customizable shapes and properties. Liu *et al.*[75] prepared an aqueous poly(3,4-ethylenedioxythiophene):poly(styrene sulfonate) ink functionalized with $Ti_3C_2T_x$ MXenes and printed flexible micro-supercapacitors with a high conductivity of 1525.8 S m^{-1} and a high EMI SE of 51.7 dB at a thickness of 295 μm. Dai *et al.*[76] created a lightweight MXene scaffold with a high conductivity of 1013 S m^{-1} and EMI SE above 60 dB by adding rGO microgels to the MXene ink. This customizable and shape-adaptive 3D printing technology enables the fabrication of self-supported rGO microgel printed structures (Fig. 4d).

Ma *et al.*[77] proposed a facile fabrication strategy for thermally conductive graphite nanosheets (GNPs)/poly(lactic acid) sheets with ordered GNPs *via* fused deposition modeling 3D printing technology. When the content of GNPs was 18.60 wt% and using four layers of $Ti_3C_2T_x$ (6.98 wt%) films, the thermally conductive and EMI shielding effectiveness of the composites significantly increased to 65 dB (3.00 mm).

Homogeneous polymer/MXene composites are widely used because of their simple preparation process. They have easy blendability and processability and can be formed by simple melt blending, solvent-assisted direct mixing,[74] and printing[75] processes. However, to achieve EMI SE values of above 20 dB, an effective conductive network of overlapping filler particles with uniform dispersion is required, which necessitates a high conductive filler content. However, this degrades their mechanical properties and processability. Homogeneous MXene/polymer composites are therefore suitable for mass-produced components with moderate EMI SE requirements.

Multilayer MXene/polymer composites

Multilayer MXene/polymer composites have been prepared by vacuum-assisted filtration, spin-coating, film scraping, gel film formation, and deposition methods. The excellent conductivity of the MXene layers means these multilayer composites have excellent EMI-shielding performance. Multilayer structures have multiple internal interfaces and interlayer structures, facilitating EMW multiple reflection losses and attenuation. Several designs have been reported, including compact alternating layer and sandwich structures, fabric structures, gradient structures, and multilayer MXene structures without a matrix phase.

Compact alternating-layer and sandwich-structured MXene/polymer EMI-shielding composites. MXene/polymer composites with compact alternating layers or sandwich structures
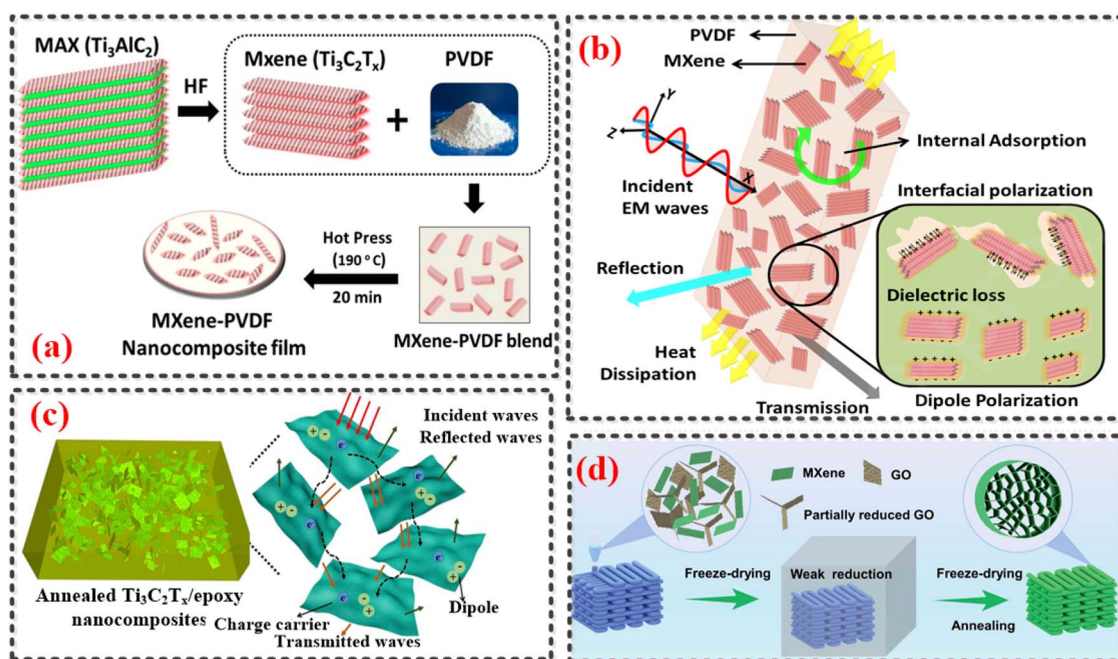

Fig. 4 Preparation and shielding mechanisms of homogenous MXene/polymer nanocomposites. (a) Preparation and (b) shielding mechanism of homogenous $Ti_3C_2T_x$/PVDF nanocomposites. Reproduced from ref. 73 with permission Elsevier Ltd., © 2019. (c) Shielding mechanism of annealed $Ti_3C_2T_x$/epoxy nanocomposites. Reproduced from ref. 70 with permission from Royal Society of Chemistry, © 2008. (d) Fabrication process of hierarchical MXene/rGO scaffolds. Reproduced from ref. 76 with permission from the Royal Society of Chemistry, © 2022.

provide multiple reflection and absorption interfaces. EMWs are predominantly reflected at interfaces with impedance mismatch. Compact structures with alternating or sandwiched layers[78] promote EMW shielding based on the multiple reflection mechanism. Additionally, the compact structure compresses the conduction space for incident EMWs while prolonging the dissipation path for reflected waves. Increasing the number of internal reflections significantly increases EMW absorption,[79,80] resulting in efficient EMI shielding even in micron-thick materials.

Shahzad et al.[37] prepared an 8 μm-thick composite comprising sodium alginate (SA) and 90 wt% $Ti_3C_2T_x$, which had an excellent EMI SE of 57 dB. Filtration is convenient for preparing compact layered MXene/polymer structures. In particular, vacuum-assisted filtration is a quick and effective technique for creating compact bilayer or multilayer MXene/polymer EMI-shielding composites. However, this approach has weak mechanical strength and insufficient interlayer adhesion. Thus, several researchers are exploring methods to achieve excellent mechanical adhesion in multilayer MXene/polymer structures for EMI-shielding materials. Ma et al.[81] used a practical two-step vacuum-assisted filtration process to create a $Ti_3C_2T_x$/AgNW aramid double-layer composite nanopaper with excellent flexibility and high mechanical strength. This was followed by hot-pressing to improve the interfacial adhesion between lamellae. A 20 wt% MXene/AgNW composite had a high conductivity of 92 200 S m^{-1} and an outstanding EMI SE of up to 80 dB. Wei et al.[82] prepared an ultrathin, lightweight, and flexible film with excellent EMI SE using a simple filtration method. The composite film had a "brick–cement" structure, where the MXene "bricks" provided EMI-shielding ability and aramid nanofiber "cement" provided mechanical strength. The $Ti_3C_2T_x$/aramid nanofiber composite film exhibited an excellent EMI SE of 34.71 dB at 8.2 GHz with a thickness of 12 μm. Liu et al.[83] investigated polyurethane (PU)/$Ti_3C_2T_x$ nanocomposite films with a highly organized nanostructure that resembles the "brick and mortar" structure of nacre. The nacre-mimetic nanocomposite films exhibited outstanding flexibility, excellent mechanical properties (tensile strength above 60 MPa, fracture toughness exceeding 2.5 MJ m^{-3}), superior electrical conductivity (4236.7 S cm^{-1}), and outstanding EMI-shielding performance (56.9 dB with 10 wt% PU and an ultra-thin thickness of 8.4 μm).

Zhou et al.[84] prepared multilayer films containing alternating cellulose nanofibers (CNFs) and $Ti_3C_2T_x$ MXene layers using an efficient vacuum extraction method. The alternating layer structure contributed to EMI shielding by a "reflection–absorption–zigzag reflection" mechanism, resulting in a high EMI SE of 40 dB in the X- and K-bands (8.2–12.4 and 26.5–40.0 GHz, respectively) (Fig. 5a). Zhang et al.[85] fabricated a sandwich-structured film using a Ca-ion-crosslinked SA montmorillonite polymer and $Ti_3C_2T_x$ MXenes (Fig. 5b). In addition to an EMI SE of 50.01 dB, the film had excellent mechanical properties (84.4 MPa) and fire resistance.

The $Ti_3C_2T_x$/polymer EMI shielding hybrid film has excellent mechanical properties. To create $Ti_3C_2T_x$/polymer EMI shielding hybrid films, layers are blended or alternated layer-by-layer.[86,87] Blending is used to create the $Ti_3C_2T_x$/polymer EMI shielding composite film, where the highly conductive $Ti_3C_2T_x$ is randomly dispersed within the insulating polymer matrix.[88] However, the blending technique requires a substantial amount of $Ti_3C_2T_x$ to create a continuous and effective conductive network, which can impact the processing and mechanical characteristics of the composite film.[89] The issue of disordered conductive networks was solved by Zhang et al.[90] who created ordered conductive networks of EMI shielding composite films and created directional porous structures using ice crystals that were directed in a specific direction. When $Ti_3C_2T_x$ is present at 80%, the resulting aerogel with a regular directional porous structure can create multiple EMW reflection losses and accomplish excellent EMI shielding performance (70 dB).

The layer-by-layer alternating $Ti_3C_2T_x$/polymer EMI shielding composite has excellent mechanical properties. The polymer layer's mechanical framing effect provides excellent mechanical properties that can prevent $Ti_3C_2T_x$ layer cracks from spreading to the rest of the composite film.[43,91] However, the multilayer structure partially destroys the $Ti_3C_2T_x$ conductance network, causing the conductivity and EMI shielding performance of the composite film to decrease.

Other methods of preparing MXene/polymer composites with compact layered structures include spin–spray-coating and hot-pressing. Notably, these composites can be tailored to achieve multiple functionalities, including light transmission. Weng et al.[92] employed a spin–spray layer-by-layer method to assemble multifunctional semi-transparent MXene/CNT composite films with high conductivities (130 S cm^{-1}) and specific EMI SE (58 187 dB cm^2 g^{-1}) owing to their sandwich assembly. Zhou et al.[93] prepared transparent, flexible, and conductive EMI-shielding films from MXene/AgNW/polymer composites by a spray–spin technique coupled with hot-pressing. The films had an EMI SE of 32 dB, resistance of 18.3 Ω sq^{-1}, and light transmission of 52.3%. Chen et al.[94] also fabricated EMI-shielding and light-transmitting MXene/AgNW multilayer films using a scalable spray-coating technique. AgNWs were incorporated into the MXene nanosheets via capillary action during water evaporation, and the loading of components within the multilayer structure was optimized. The macroscopic layered structure had an EMI SE of 49.2 dB and a high light transmittance of 83%. A film with a high EMI SE of 96.5 dB and light-transmittance of 59% was also prepared.

Multilayer composites with alternating layers of poly(vinyl alcohol) (PVA) and MXenes fabricated by casting provide a compact network for conducting heat and electrons.[95] The multilayer PVA/MXene composite had an excellent EMI SE of 44.4 dB at a thickness of 27 μm (Fig. 5c). By etching 2D MXene nanoribbons with sulfuric acid, Ying et al.[96] created defects or dislocations in the MXene nanoribbons. As the density of defects and dislocations increased, the internal tension within the MXene film increased, resulting in the formation of natural wrinkles. According to Kelvin probe force microscopy and first-principles calculations, the formation of wrinkles induces the formation of electric dipoles on the film surface during wrinkle induction, which significantly increases the material's ability to absorb incident EMWs. After that, the folded film was stacked

Fig. 5 Preparation and properties of MXene/polymer EMI shielding composites with multilayer structures. (a) "Reflection–absorption–zigzag reflection" mechanism of a multilayer CNF@MXene film prepared by vacuum extraction. Reproduced from ref. 84 with permission from the American Chemical Society, © 2020. (b) Sandwich films prepared by vacuum-assisted filtration. Reproduced from ref. 85 with permission from the American Chemical Society, © 2020. (c) PVA/MXene films fabricated by multilayer casting. Reproduced from ref. 95 with permission from Elsevier B.V., © 2019. (d) Intelligent fabric is prepared by coating polyaniline/MXene layers on a fabric substrate. Reproduced from ref. 102 with permission from the American Chemical Society, © 2022. (e) CNT/MXene/CNF composite paper with a gradient and sandwich structure prepared by a facile alternating vacuum-assisted filtration technique. Reproduced from ref. 105 with permission from The Authors, © 2019.

to obtain a minimum thickness of 20 μm, resulting in high-performance EMI SE (107 dB). The presence of electric dipoles increased the absorption of EMWs.

Wang et al.[97] constructed layered- and sandwich-structured composites comprising polyacrylonitrile@TiO$_2$ and Ti$_3$C$_2$T$_x$ films via a simple solution dip-coating method, which had an average EMI SE of 32 dB at 45 μm.

Compact MXene/polymer composites comprising self-supporting MXenes constructed by vacuum-assisted filtration or scraping of 2D MXene flakes are extremely important macro-assemblies. They display unique EMI shielding benefits and EM and physicochemical properties. However, the strong van der Waals and hydrogen bonding interactions between MXene layers lead to a tightly stacked structure, which reduces the space between layers[98] and significantly shortens the EMW transmission path, reducing the interaction of EMWs with the material. Thus, the absorption losses and total EMI SE are reduced. Furthermore, the specific surface areas of stacked MXene sheets[98] are far lower than theoretical expectations, and the active sites on the MXene lamellae are greatly reduced; therefore, they do not provide the full advantages of MXenes.

Multilayer fabric structures as EMI-shielding materials. MXene/polymer composites with multilayer fabric structures can be produced by dipping, deposition,[99] and coating methods. Wang et al.[100] prepared $Ti_3C_2T_x$-decorated polyester fabrics by the deposition of polypyrrole-modified $Ti_3C_2T_x$ sheets. The conductivity and stability of the $Ti_3C_2T_x$ sheets were effectively improved by the presence of polypyrrole. A single-layered polypyrrole/$Ti_3C_2T_x$/polyester fabric had an EMI SE of 42 dB, increasing to 90 dB with three layers.

Geng et al.[101] prepared an EMI-shielding fabric for use in protective clothing and flexible wearable smart devices by loading $Ti_3C_2T_x$ sheets onto cotton fabric for enhanced EMW absorption. The fabric had high electrical conductivity (1570 S cm^{-1}) and an outstanding EMI SE (50 dB at 2–18 GHz). Li et al.[102] demonstrated a polyaniline/MXene intelligent fabric composite with an excellent EMI SE of 54 dB at a thickness of 440 μm after optimizing the composition and dosage (Fig. 5d). Lan et al.[103] adopted a stepwise assembly technique using alternating layers of MXenes and insulating polymers to prepare a fire-resistant EMI-shielding material. Guo et al.[104] fabricated a hierarchically multifunctional polyimide (PI) composite film using a hierarchical design and assembly strategy. It integrates excellent EMI shielding (34.0 dB), good tensile strength (93.6 MPa), and high in-plane thermal conductivity coefficient (95.40 W mK^{-1}) with 61.0 wt% GO/expanded graphite and 23.8 wt% Fe_3O_4/PI. Multilayer MXene/polymer fabrics exhibit good conductivity and flexibility,[101] and extend their functionality beyond EMI shielding. Notably, when used in clothing, they can directly protect people from strong EM fields. However, due to limitations in fabricating multilayer MXenes, the conductive material mostly exists on the surface of the fabric, and the weak interfacial bonds between the functional layer and fabric mean they can easily separate, hindering the effectiveness of MXene/polymer fabrics for EMI shielding in practical applications.

Due to impedance mismatch, ultrahigh-conductivity EMI-shielding fabrics mainly shield EMWs by reflection. In view of this, multilayer MXene/polymer composites with gradient structures are promising, because the gradient structure improves the wave impedance at the composite/air interface, thereby enhancing EMW absorption and ultimately improving the overall EMI SE.

Gradient multilayer structure MXene/polymer composites. Multilayer structures formed from polymers with gradated amounts of conductive filler do not have large differences in dielectric constant at the interfaces, which reduces EMW reflection and results in excellent EMW absorption. Cao et al.[105] constructed an ultrathin flexible CNT/MXene/CNF composite paper with a gradient sandwich structure using alternating vacuum-assisted flotation (Fig. 5e). The electrical conductivity (2506.6 S m^{-1}) and EMI SE (38.4 dB) of the paper were promising. Moreover, the layered structure provided excellent transparency, flexibility, and mechanical properties.[67,106]

Composites with layered structures can show excellent EMI-shielding performance.[37] Moreover, those with gradient structures can regulate the contributions of EMW reflection and absorption. Gradient structures have little influence on the EMI-shielding performance of composites; however, they can significantly improve the wave impedance between the composite and free space, resulting in a notable increase in the EMW absorption performance,[107] which is significant for achieving absorption-dominated EMI-shielding. In addition, gradient structures provide prolonged dissipation paths for incident and internally reflected waves and a unique low reflection–absorption–high reflection–reabsorption EMW dissipation mechanism.[107] This enhanced EMW absorption performance is the reason for the high EMI-shielding ability of gradient MXene/polymer composites. However, from the perspective of electrical performance, the interlayer conductive network in gradient structures is discontinuous, which affects the electron transmission and EMI SE. In addition, the mechanical properties of multilayer gradient composites are inadequate, because improving the interfacial forces and transitions between gradient layers tends to have been neglected in current research. Thus, the interlayer interactions are relatively weak. The poor mechanical properties of these materials greatly restrict their application as EMI-shielding materials.[82] One way to overcome this drawback is to develop multilayer gradient composites with more robust structures. To achieve this, candidate matrices such as PI[108] should be considered to protect the MXene layers from mechanical stress along with suitable processing conditions.

Overall, multilayered MXene/polymer composites[109] have an excellent ability to block incoming EMWs, significantly reduce EMI, and provide a protective effect. Multilayer structures with different functional layers produce composites with multifunctional properties.[102] Nevertheless, as the impedance mismatch between the composite surface and free space increases, the shielding material will reflect increasing amounts of EMWs, causing secondary EMW pollution. However, the use of electrically insulating polymers results in large insulating gaps between adjacent MXene flakes that disrupt the electron conduction path, preventing the formation of MXene-based layer-by-layer architectures with high electrical conductivity.[110]

Porous MXene/polymer composites

The stacking of MXenes in layered structures prevents EMWs from penetrating these dense films, which decreases EMW

absorption and thus impairs further improvement of the EMI SE.[111] To increase the contribution of multiple internal reflections toward EMW absorption,[112] MXene/polymer composites with porous structures have been designed. Porous 3D structures are divided into (1) porous MXene structures without a polymer matrix; (2) prefabricated porous MXene structures backfilled with a polymer; and (3) porous polymers into which MXenes are deposited.

Porous MXene structures without a polymer matrix

Porous MXene structures without a polymer matrix benefit from the unique advantages of porous structures in regulating the conductivity and dielectric constant. Furthermore, the EMI SE is enhanced by repeated absorption and reflection losses within the structure. MXene foams with porous structures can effectively attenuate incident EMWs.[113] Moreover, they are lightweight and highly conductive.

Polymer-free porous MXene structures have been prepared by ice-templating, gas foaming, hydrothermal assembly, and sacrificial polymer-templating methods. Bian et al.[114] fabricated ultralight MXene aerogels with an excellent EMI SE (75 dB) and extremely low EMW reflection (1 dB) by ice-templating. The aerogels readily absorbed organic solvents owing to their microsized pores, which were created as a result of the morphology of the ice crystals. Wang et al.[115] prepared a flexible and ultralight carbon foam/$Ti_3C_2T_x$ hybrid by vacuum impregnation and freeze-drying. The flexible and compression-resilient material had a minimum reflection loss of 45 dB with 9.8 wt% $Ti_3C_2T_x$.

MXene surfaces are rich in hydrophilic groups. To avoid a reduction in EMI SE in humid environments, Liu et al.[116] fabricated an MXene foam with elevated electrical conductivity, ultrahigh strength, and excellent hydrophobicity by a hydrazine foaming process (Fig. 6a). The EMI SE (70 dB) of the MXene foam was significantly higher than that of an un-foamed MXene membrane (53 dB) of the same quality.

Self-assembly and sacrificial templating are ingenious methods for preparing porous MXenes. Li et al.[117] synthesized lightweight and free-standing core/shell rGO/$Ti_3C_2T_x$ heterojunction foams (Fig. 6b). In addition to the connectivity between the core and shell, the heterogeneous interface resulted in controllable complex permittivity. The hybrid foam had excellent EMW absorption, thus achieving the best possible EMI-shielding performance.

Porous MXene structures without polymer matrices have been designed with excellent elasticity and conductivity. For example, a superelastic anisotropic aerogel with outstanding thermal insulation capabilities was created by Deng et al.[118] using $Ti_3C_2T_x$ MXenes and acidified CNTs (Fig. 6c). The aerogel with 5 wt% acidified CNTs had ultra-elasticity, minimal plastic deformation, and good fatigue compression resistance. Moreover, it had a conductivity of 447.2 S m^{-1} and X-band EMI SE of more than 51 dB in a paraffin matrix at a density of 9.1 mg cm^{-3}. The average EMI SE was enhanced to 90 dB by increasing the density to 18.2 mg cm^{-3}.

The porosity of MXene structures without a polymer matrix increases the complexity of the internal structure, prolonging the

EMW propagation path[119] and increasing the probability of refraction and scattering. This is conducive to EMW attenuation and dissipation, resulting in excellent EMI SEs. Heterostructures, boundaries, stacking faults, and surface functional groups of MXenes and multiphase materials with different permittivities enhance the dielectric properties synergistically,[120] optimizing the impedance matching of the composite and effectively enhancing EMW absorption. Their flexibility, light weight, and superior EMI SE mean that MXene foams have clear prospects for aerospace and portable/wearable smart electronics applications. Nevertheless, MXene structures without a polymer matrix have low mechanical properties owing to the weak interactions between MXene layers, and they cannot be bent or squeezed, which greatly limits their practical applications.[121] Thus, MXenes are usually compounded with polymers to prepare composites with excellent mechanical properties and good EMI SE.

Backfilling polymers into a prefabricated MXene porous structure. Increasing the filler (MXene) content improves the EMI-shielding performance of polymer/MXene composites; however, owing to the extremely high yield strength of the filler particles, high filler contents deteriorate the mechanical properties.[122] Regulating the dispersion of filler particles is therefore a suitable means of obtaining higher EMI SEs at lower filler loadings (1.90 vol% MXene).[123] Composite materials with 3D networks and low filler loadings improve the EMI SE by interfacial polarization and multiple reflection losses of EMWs. The preferred method of obtaining composites with elevated conductivity is to fill a preconstructed conductive network with a polymer.[124,125] Notably, this method ensures the integrity of the conductive network and enables the percolation threshold to be met at a low filler content. This post-filling method facilitates the production of a strong conductance network and greatly improves the utilization of this network to achieve excellent EMI SE with versatile material design.

Zhao et al.[126] prepared epoxy/MXene/rGO hybrid aerogels by a hydrothermal method with freeze-drying technology. The epoxy nanocomposite had strong electrical conductivity (695.9 S m^{-1}) and excellent EMI resistivity (X-band EMI SE of over 50 dB at a low $Ti_3C_2T_x$ content of 0.74 vol%). Wu et al.[127] prepared a 3D MXene aerogel from a SA and MXene dispersion. The MXene aerogel was then dip-coated with polydimethylsiloxane (PDMS) to improve the stability and durability of the porous structure. The coating also improved the 3D conductive network. The PDMS-coated MXene aerogel had an excellent EMI SE (70.5 dB) and good conductivity (2211 S m^{-1}) (Fig. 6d). Wang et al.[128] fabricated a 3D electroconductive CNF/$Ti_3C_2T_x$ MXene aerogel with aligned pores by directional freezing followed by freeze-drying. The nanocomposite had an EMI SE of 74 dB, high thermal resistance, and conductivity of 1672 S m^{-1}.

Backfilling polymers into a prefabricated MXene porous structure is a notable method of improving the mechanical properties of EMI-shielding composites. In another study, Wang et al.[129] fabricated 3D hybrid $Ti_3C_2T_x$/carbon-foam/epoxy nanocomposites by a sol–gel process with vacuum-assisted impregnation followed by thermal reduction (Fig. 6e). The nanocomposite had excellent mechanical properties, optimal electrical conductivity (184 S m^{-1}), and high X-band EMI SE (46 dB).
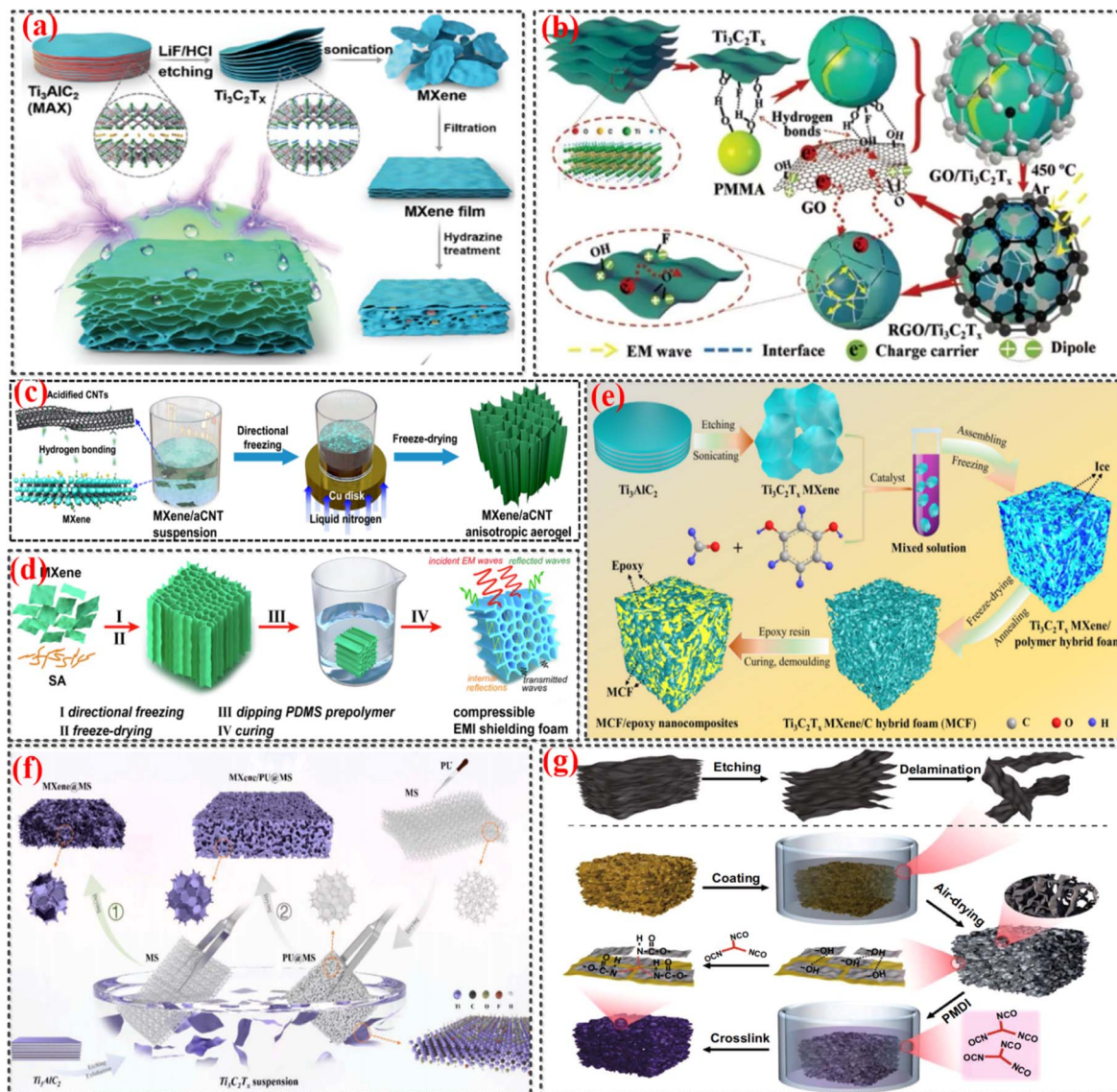
Fig. 6 (a) MXene foam fabricated by hydrazine foaming process. Reproduced from ref. 116 with permission from Wiley-VCH Verlag GmbH & Co. KGaA, Weinheim, © 2017. (b) Sacrificial templating method for the fabrication of rGO/Ti$_3$C$_2$T$_x$ core/shell composites with a hollow spherical structure. Reproduced from ref. 117 with permission from Wiley-VCH Verlag GmbH & Co. KGaA, Weinheim, © 2018. Preparation of porous MXene structures for EMI-shielding applications. (c) Ti$_3$C$_2$T$_x$ MXene/acidified CNT anisotropic aerogel. Reproduced from ref. 118 with permission from the American Chemical Society, © 2021. (d) Backfilling PDMS into a prefabricated MXene porous structure. Reproduced from ref. 127 with permission from Elsevier B.V., © 2020. (e) 3D hybrid Ti$_3$C$_2$T$_x$ MXene/carbon-foam/epoxy nanocomposite fabricated by a sol−gel and thermal reduction process. Reproduced from ref. 129 with permission from The Authors, © 2019. (f) Polymer bubbles with deposition of MXenes to form a hybrid MXene/PU@MS porous structure. Reproduced from ref. 132 with permission from Elsevier B.V., © 2021. (g) Porous PI composite coated with Ti$_3$C$_2$T$_x$ MXenes. Reproduced from ref. 133 with permission from The Authors, © 2022.

Depositing or inserting MXenes into prefabricated porous polymers. Lightweight MXene/polymer composites can also be prepared by depositing or inserting MXenes into a prefabricated porous polymer, such as a lightweight polymer composite.[130] The conductivity and dielectric parameters[120] of the composite can be optimized by introducing MXenes into the porous structure, thereby increasing the impedance matching and encouraging EMWs to enter the structures, where they then encounter multiple internal reflections.[12] The porous structure further amplifies the EMW dissipation capacity.[131] By

enhancing the conductive and polar losses of EMWs, such porous MXene/polymer composites can achieve excellent EMI shielding and EMW absorption. Moreover, continuous conductive networks of MXenes are more easily achieved by dipping a prefabricated porous polymer into an MXene solution than by backfilling the polymer into a porous MXene network.

Ma *et al.*[132] prepared a lightweight, flexible, and self-healing EMI-shielding sponge from a prefabricated 3D porous polymer skeleton and MXene flakes by a simple dip-coating method (Fig. 6f). To form the MXene film, the PU-coated sponge was

immersed in an MXene dispersion to create a coating on the porous skeleton. The composite sponge had an X-band EMI SE of 90.49 dB with an extremely low $Ti_3C_2T_x$ loading (0.82 vol%), with absorption-dominated (93%) shielding. Zeng et al.[133] demonstrated a lightweight, ultra-flexible, and robust $Ti_3C_2T_x$-coated PI porous composite. Owing to the intrinsic conductivity of $Ti_3C_2T_x$ and interfacial polarization losses of PI, the composite had a satisfactory X-band EMI SE of 62.5 dB (Fig. 6g).

A multifunctional EMI-shielding skin for wearable electronics and robotics applications was demonstrated by Nguyen et al.[134] $Fe_3O_4@Ti_3C_2T_x$/graphene/PDMS composites were obtained by growing graphene on Ni foam by chemical vapor deposition, followed by the deposition of Fe_3O_4-intercalated $Ti_3C_2T_x$, PDMS coating, and etching to remove the original Ni framework. Remarkable EMI SE values of 80 and 77 dB were achieved in the X- and K-bands, respectively, owing to the excellent EMW absorption efficiency.

Porous MXene/polymer composite structures have two main advantages for EMI shielding. First, the pores reduce the density of the material, resulting in a lightweight composite. Regulating the dispersion of conductive filler balances the density of the material with the conductivity. Second, numerous interfaces are enriched inside the material, which enhances the polarization and dielectric losses and ultimately the EMI SE. The air contained in the pores reduces EMW reflection at the surface of the material while increasing EMW absorption,[116] which effectively prevents EM leakage.[36,135]

However, porous MXene/polymer composites have several shortcomings. Research on the effect of the microstructure on the EMI-shielding performance is lacking, especially the relationship between the pore size and the EMI-shielding mechanism. Furthermore, achieving multifunctional polymer nanocomposites with excellent EMI SEs at low MXene loadings remains a great challenge. It is necessary to simplify the preparation process of porous MXene/polymer composites. Thus, realizing lightweight multifunctional MXene/polymer porous EMI-shielding materials with high strength, thermal resistance, flame retardance, and other functionalities is a key future research and development trend.

Segregated MXene/polymer composites

Segregated MXene/polymer composites overcome the disadvantages of homogeneous structures with random dispersions of conductive fillers. Homogeneous EMI-shielding materials require larger amounts of conductive filler to meet the higher percolation thresholds, which is counterproductive to achieving lightweight materials. In contrast, in segregated polymer composites, the conductive filler particles have a controlled distribution, rather than being randomly dispersed throughout the matrix. Conductive MXenes concentrate at the surface of the polymer matrix, which greatly increases their density along defined conductive pathways, thus reducing the percolation threshold.[136] Consequently, more conductive and compact networks can be achieved.[137]

The polar functional groups at the surface of MXene flakes mean they are hydrophilic.[57] Therefore, electrostatic interactions are typically necessary during aqueous-phase preparation to achieve uniform dispersions and create complete conductive networks in segregated composites.[109] Sun et al.[123] deposited negatively charged MXene nanosheets onto positively charged polystyrene microspheres by electrostatic assembly followed by compression molding (Fig. 7a). Owing to the high conductivity and efficient conductive network of MXenes, the prepared nanocomposites had a low percolation threshold (0.26 vol%), excellent conductivity (1081 S m^{-1}), and outstanding EMI SE (>54 dB).

Using the electrostatic self-assembly of MXenes on natural rubber (NR) microspheres followed by vacuum filtration, Luo et al.[138] prepared flexible MXene@NR films with segregated structures (Fig. 7b). Electrostatic repulsion forces enabled the MXene sheets to selectively distribute on the NR particle surfaces, thus creating an interconnected network that facilitated electron transport and load transfer at low MXene concentrations. In addition to efficient electronic conductivity, the segregated structure effectively dissipated external stresses. With a loading of 6.71 vol% MXenes, the MXene@NR films exhibited excellent conductivity (1400 S m^{-1}) and EMI SE (53.6 dB). In another study, Ma et al.[139] used flocculation-assembled $Ti_3C_2T_x$ nanosheets as an interfacial solder to achieve ultra-efficient EMI shielding and anti-dripping performance during burning. Selective heating with microwave-induced diffusion was used to construct segregated $Ti_3C_2T_x$/polypropylene composites with a continuous and compact network (Fig. 7c). After sintering, the composites exhibited extremely high X-band EMI SE at a low $Ti_3C_2T_x$ loading of 1.138 vol%. A similar method was used to fabricate segregated poly(ethylene-co-octene)/CNT composites with promising EMI-shielding performance.[140] Microwave-assisted sintering has also been used to fabricate segregated polyetherimide/CNT composites with high EMI-shielding performance.[141]

MXene/polymer composites with segregated structures have a relatively complete 3D conductive network and rich cellular-like interface that introduces a large number of conductive interfacial layers. In these composites, some EMWs are reflected due to impedance mismatch,[73] while the conductive network absorbs and attenuates the EMWs.[80] The residual EM energy interacts with the conductive network, producing strong eddy current losses and transforming the EM energy into heat energy.[52] EMI-shielding composites with segregated structures have significant advantages, including low packing, high conductivity, multiple interfacial reflections, and high EMW absorption.[137]

The obvious drawback of segregated structures is the reduction of mechanical properties due to weak bonding between the filler and matrix. The polymer phase is dispersed in a conductive network of inorganic filler particles. Essentially, the conductive filler particles are selectively dispersed at the interface of the polymer phase and microscopic defects inevitably form. This means that the composite does not retain the excellent mechanical properties of intact polymers.[142] The poor bonding between the filler and matrix phases makes it challenging to prepare segregated composites with high mechanical strength.[142] To overcome this drawback, Xu et al.[140] prepared
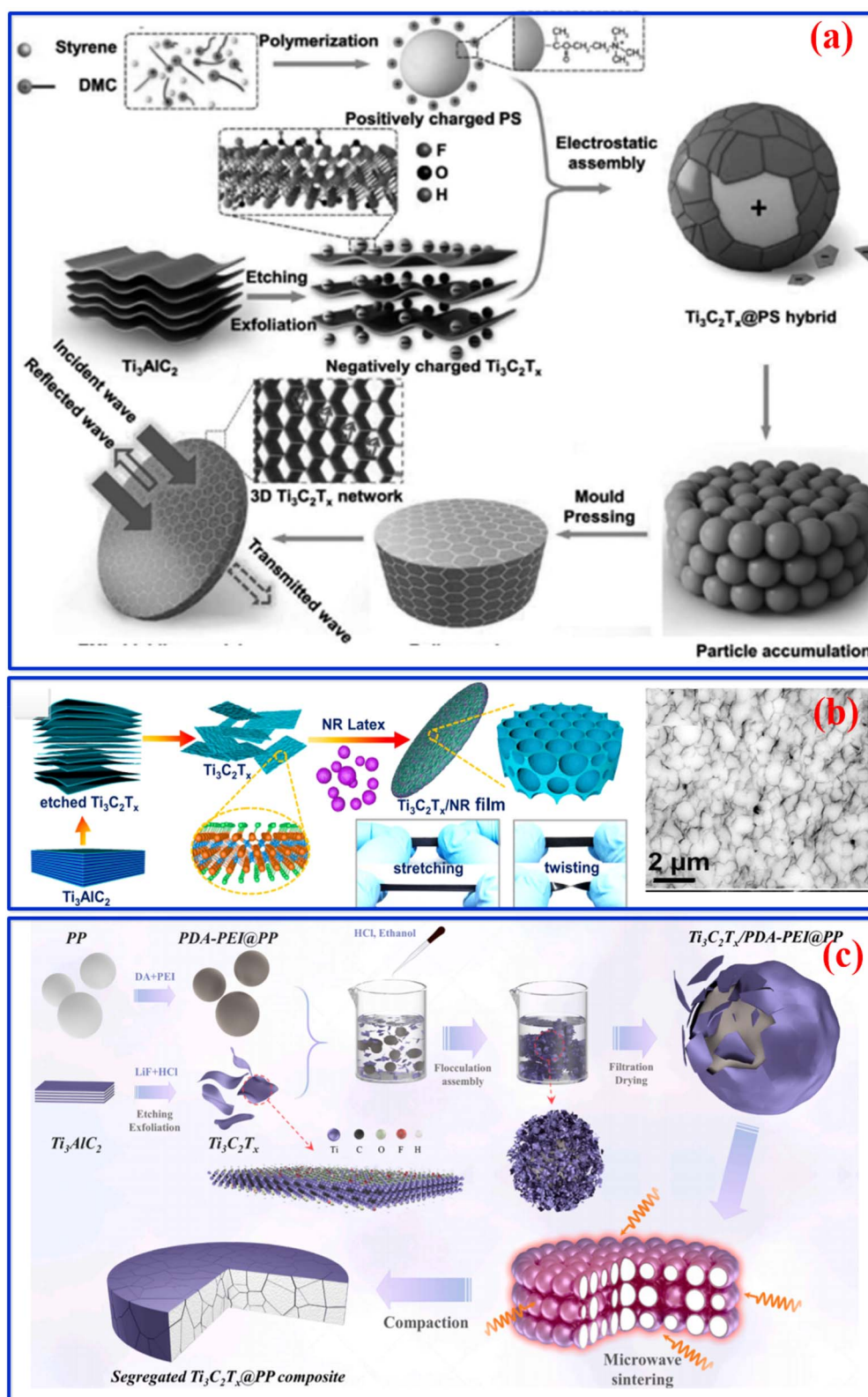
Fig. 7 Fabrication of MXene/polymer composites with segregated and hybrid structures. (a) Segregated $Ti_3C_2T_x$/polypropylene composite. Reproduced from ref. 123 with permission from Wiley-VCH Verlag GmbH & Co. KGaA, Weinheim, © 2017. (b) Segregated MXene@NR film. Reproduced from ref. 138 with permission from Elsevier Ltd., © 2019. (c) Segregated $Ti_3C_2T_x$@polystyrene nanocomposite. Reproduced from ref. 139 with permission from Elsevier B.V., © 2021.
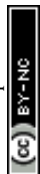
segregated polymer/CNT EMI-shielding composites with enhanced mechanical properties by selective microwave sintering. Microwave sintering caused the rearrangement and dispersion of agglomerated CNT fillers in the interface region, which absorbed large amounts of energy and promoted stress transmission.

One possible way to overcome this problem is to enhance the interface binding between the MXene nanosheets and the polymer matrix.[143] This can be achieved by modifying the surface terminations of MXene nanosheets with functional groups that can interact with the polymer chains.[144] Carboxyl groups can improve the interfacial adhesion between MXene and the polymer. Another possible way is to combine different types of polymers with MXene nanosheets to achieve a balance between flexibility, toughness, and strength.[145]

Hybrid structures

The term "hybrid material" has broad meanings.[146] In the case of EMI-shielding materials, hybridity refers to the use of multiple structural design features within a single material. No single structural feature is able to meet the increasingly stringent requirements for EMI shielding, but hybrid structures incorporate the advantages of multiple structural features to construct more complete conducting networks and conducting–insulating interfaces, and thus achieve stronger polarization and conduction losses,[147] and ultimately increase the EMI SE.

Weng et al.[148] designed a lightweight hierarchical AgNW/MXene/melamine formaldehyde sponge composite with a multilayer/porous hybrid structure to increase the multiple reflection losses and scattering of EMWs. AgNWs and MXene suspension were deposited layer-by-layer in the pore channels of the polymer sponge, and the MXene suspension formed an irregular honeycomb structure upon freeze-drying (Fig. 8a). This hybrid structure achieved an EMI SE of 52.6 dB owing to its hierarchical structure, which increased multiple reflections and scattering of EMWs. The mechanism of EMW attenuation is similar to that of layered composites with conductive fillers.

Cheng et al.[108] produced a hierarchically porous PI/Ti$_3$C$_2$T$_x$ film with stable EMI shielding and strong mechanical properties under extreme conditions. The film was formed by a unidirectional aerogel-assisted immersion process by hot-pressing. The PI/Ti$_3$C$_2$T$_x$ aerogel was clamped between two stainless steel plates under a force of 200 N in a vacuum oven at 300 °C for 30 min (Fig. 8b). The conductive path of the Ti$_3$C$_2$T$_x$ sheets provided high reflection losses and high conductivity, and the layered porous structure created multiple interfaces to prolong the EMW propagation path and facilitate interfacial polarization losses. At a thickness of 90 μm, an absolute EMI SE of 15 527 dB cm m^{-2} was achieved with only 2.0 vol% Ti$_3$C$_2$T$_x$. A gradient porous PI/Ti$_3$C$_2$T$_x$ film also had excellent EMI-shielding properties. After exposure to harsh conditions (humidity, high and low temperatures, and rapid thermal shock), the film still functioned properly.

Jia et al.[149] designed a hybrid polymer/MXene composite with porous, segregated, and gradient multilayer structural features.

They prepared polyaniline-modified polypropylene foam beads by impregnation, oxidation, and decoration, then assembled them into 3D stacks and encapsulated them in PDMS with an MXene network (Fig. 8c). A good EMI SE of 39.8 dB was achieved with just 0.0449 vol% MXene. The use of a gradient structure and selective dispersion of conductive filler provides insight into the design of advanced EMI-shielding composites.

In short, to build more complete conducting networks and more conductive–insulating interfaces, and thus achieve stronger interfacial polarization,[150] dipole polarization,[133] and conduction losses, hybrid structures are used to best exploit the advantages and bypass the drawbacks of different structural features. Overcoming the shortcomings of single-structure designs gives full play to the efficiency of each component and improves the EMI SE. However, overly complex hybrid structures are not the best choice for EMI-shielding composites owing to the complexity of their preparation. Nonetheless, a multifunctional and complex hybrid structure may be more suitable for demanding EMI shielding environments.

Magnetic/conductive MXene/polymer composites

Magnetic fillers can be added to conductive MXene/polymer composites[151,152] to achieve impedance matching and increase the absorption of incident EMWs. It is well accepted that both magnetic and dielectric losses consume EMWs effectively.[153] Huang et al.[11] prepared a magnetic/conductive MXene/polymer composite that exhibited excellent EMI absorption performance based on magnetic losses. This confirmed that magnetic/conductive MXene/polymer composites have great potential for energy conversion and EMI-shielding applications.[154] Jiang et al.[155] demonstrated a Fe$_3$O$_4$-functionalized graphene nanoplate composite with good absorption of X-band EMWs due to its high impedance matching. Wang et al.[156] also confirmed this result.

Common methods of adding a magnetic phase include decorating and blending the conductive filler with magnetic material before adding it to the composite. However, this can actually decrease the conductivity and EMI SE. The addition of non-conductive Fe$_3$O$_4$ tends to block the conductance path,[157] leading to a large drop in the electrical conductivity. Shen et al.[49] reported that magnetic fillers can significantly reduce the electrical conductivity of composites, and confirmed that the magnetic filler blocks the conductance path. Raagulan et al.[158] prepared MXene/oxidized CNT nanocomposites and demonstrated a maximum conductivity of 16.32 S cm^{-1} between the MXene[44] and oxidized CNT composites (maximum value of 8.84 S cm^{-1}). The conductivity is affected by the mixture. Zhan reported that[10] as the magnetic component increased, the electrical conductivity gradually declined from 438 to 161 S cm^{-1}.

A promising strategy for introducing magnetic phases into conductive MXene-based composites is to segregate the conductive and magnetic filler phases to ensure that the magnetic filler does not affect the conductivity while also providing magnetic losses. To increase the magnetic losses of EMWs in Ti$_3$C$_2$T$_x$/polymer composites without affecting the
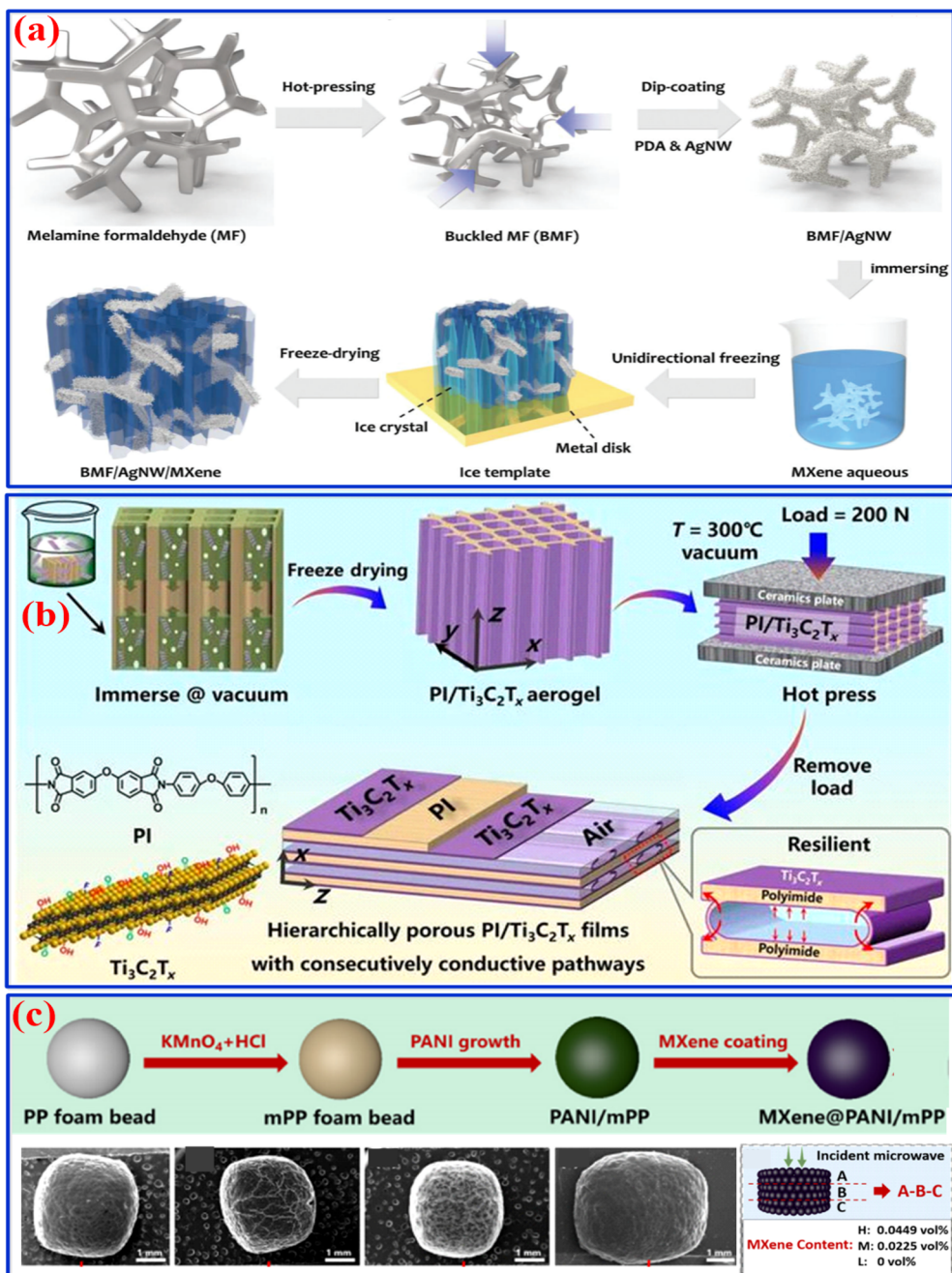
Fig. 8 (a) Buckled melamine formaldehyde sponges coated with AgNW/MXene hybrid hierarchical composite. Reproduced from ref. 148 with permission from the Royal Society of Chemistry, © 2019. (b) Hierarchically porous PI/Ti$_3$C$_2$T$_x$ composite. Reproduced from ref. 108 with permission from the Authors, © 2021. (c) MXene network decorated with polypropylene foam beads. Reproduced from ref. 149 with permission from Elsevier Ltd., © 2020.

conductivity, Liang et al.[159] modified few-layer Ti$_3$C$_2$T$_x$ nanoflakes with magnetic one-dimensional Ni chains by polyvinylpyrrolidone templating. Multiple layers of Ni particles, Ti$_3$C$_2$T$_x$ MXenes, and wax were mixed to form a three-phase composite. With 50 wt% Ti$_3$C$_2$T$_x$ and 20 wt% Ni, the EMI SE reached 66.4 dB at a thickness of 2.88 mm. The EMI SE was improved due to the contribution of magnetic loss. The magnetic particles effectively converted EM energy into heat energy via domain wall migration, ferromagnetic resonance,

and expansion of the magnetic coupling space. Simultaneously, the MXene and magnetic fillers provided a large number of reflective interfaces to achieve dielectric interfacial dissipation. Combining materials with dielectric and magnetic losses eliminates the problems associated with high filler loadings and thickness and expands the effective shielding bandwidth. Several EMI-shielding mechanisms operate simultaneously, allowing the EMI-shielding parameters to be tailored for a given application.[159] Wang et al.[160] used a similar method to produce

composite films from Ni chains, $Ti_3C_2T_x$, and PVDF. The Ni chains formed a 3D conductive network in the PVDF matrix. With 10 wt% Ni and 10 wt% $Ti_3C_2T_x$, the film had an EMI SE of 34.4 dB. In contrast, with 20 wt% $Ti_3C_2T_x$, the EMI SE dropped drastically to <1 dB. Therefore, introducing a magnetic component into $Ti_3C_2T_x$/polymer composites with dielectric losses significantly improves the EMI SE.

The structural design of magnetic/conductive MXene/polymer composites further improves the EMI-shielding performance. Song et al.[161] prepared rubber composites with magnetic Fe_3O_4 nanoparticles (Fig. 9a). The Fe_3O_4@$Ti_3C_2T_x$/3,4-dihydroxyphenylacetic acid epoxidized NR elastomers had a high X-band EMI SE of 58 dB. Moreover, the strong interfacial interactions between ligands led to a significant improvement in mechanical properties. Wang et al.[162] developed a hybrid aerogel by incorporating functionalized $Ti_3C_2T_x$ nanosheets and magnetic $NiFe_2O_4$ particles into aqueous PU. The synergistic effects of the oriented porous structure and heterostructure provided this hybrid aerogel with an EMI SE of 64.7 dB at a density of 38.2 mg cm^{-3}. Hu et al.[163] used a facile electroless plating technique to fabricate functional core@shell $Ti_3C_2T_x$@Ni particles in which thin Ni layers sandwiched $Ti_3C_2T_x$ flakes (Fig. 9b). $Ti_3C_2T_x$@Ni/wax composites with 60 and 80 wt% $Ti_3C_2T_x$@Ni had EMI SEs of 43.12 and 74.14 dB, respectively. Liang et al.[164] fabricated NiCo/MXene/CNT composite films with an EMI SE of 90.7 dB at a thickness of 53 mm owing to the combination of magnetic NiCo/MXene, highly conductive CNTs, and a compact layered structure (Fig. 9c).

Similarly, Wen et al.[165] employed a serialization strategy to reshape MXene into a 3D microsphere, providing a substrate for the directional growth of Ni nanospikes. This structural feature can provide a large number of accessible active surfaces, effectively enhancing the dielectric loss capability, and the introduction of magnetic Ni nanospikes can enable additional magnetic losses. These advantages make the synthesized 3D MXene@Ni microspheres exhibit excellent microwave absorption performance, with a minimum reflection loss value (RL) of −59.6 dB at ultra-thin thickness (∼1.5 mm) and an effective absorption bandwidth of 4.48 GHz.

These results confirm that combining materials with magnetic and dielectric losses effectively improves the EMI shielding performance owing to the layered dense stacking magnetic (NiCo/MXene) and highly conductive (CNTs) structure.

Conversely, Ma et al.[166] proposed that introducing magnetic particles was insufficient for enhancing the EMW absorption ability. They constructed a CNF/MXene/FeCo gradient composite film with double gradients in conductivity. The double gradient structure increased the EMW absorption losses from 48.6 to 53.8 dB, while the reflection losses decreased from 7.4 to 4.2 dB. The magnetic losses generated by FeCo contributed significantly to the EMW absorption capacity, while the EMW absorption capacity was also significantly enhanced by the double gradient structure.

The addition of magnetic materials greatly improves the dielectric losses of a conductive network and also introduces magnetic loss mechanisms such as natural and eddy current losses. In addition, the particles provide several heterogeneous interfaces, which is conducive to the multiple reflection and absorption losses of EMWs. Because their conductivities differ, asymmetrically distributed space charges accumulate at the $Ti_3C_2T_x$/magnetic filler interface. In addition, the impedance mismatch at the $Ti_3C_2T_x$/magnetic filler interfaces serves to reflect EMWs, resulting in multiple internal reflection losses. Strong interfacial polarization[74] and dielectric losses also occur at the interface, distributing the EMW energy. Consequently, magnetic/conductive MXene/polymer composites maintain good conductivity to provide excellent dielectric losses combined with magnetic losses. Thus, this structural design can enhance EMW absorption. However, reasonably balancing the dielectric and magnetic loss capacities by impedance optimization is a significant challenge that hinders the EMW absorption/shielding performance.[167]

Electromagnetic parameters and impedance matching for the absorption-dominated electromagnetic interference shielding of MXene/polymer composites

Electromagnetic parameters of MXene/polymer composites

EM parameters play a significant role in determining the performance of EMI-shielding materials. The absorption of EMWs is primarily influenced by the dielectric and magnetic losses[168] that arise from the permittivity and permeability of MXene/polymer composites. These properties can be represented by the real (ε') and imaginary (ε'') parts of the complex permittivity, as well as the real (μ') and imaginary (μ'') parts of the complex permeability. The magnitude of dielectric losses (tan $\delta_\varepsilon = \varepsilon''/\varepsilon'$) and magnetic losses (tan $\delta_\mu = \mu''/\mu'$), as well as the permittivity and permeability of the composites, are commonly used to assess the mechanism of EMW attenuation in MXene/polymer composites.

The permittivity of MXene/polymer composites, particularly MXene/PVDF composites, increases with increasing MXene load within a certain range.[169] This continuous increase in the dielectric is mainly due to the formation of microscopic dipoles on the surface between the MXene filler and polymer matrix under the external applied electric field, which causes accumulation.[119] Tu et al.[170] proposed that the enhancement of dielectric constant is mainly attributed to the formation of microscopic dipoles through charge accumulation at the MXene/polymer interface.

According to Luo et al.,[171] the increase in permittivity with increasing MXene loading is related to the increased probability of connection between MXene sheets. However, at higher MXene concentrations, the increased connections between MXene sheets increase the leakage current, resulting in a decrease in the permittivity.[170] This trend is reflected in Fig. 10a. The attenuation mechanism is thought to gradually shift from jump migration losses between nanosheets to relaxation losses within single nanosheets.[171]

Fig. 9 Fabrication of magnetic/conductive MXene/polymer composites for EMI shielding. (a) $Fe_3O_4@Ti_3C_2T_x$/3,4-dihydroxyphenylacetic acid epoxidized NR elastomer nanocomposite with interconnected isolation structure fabricated *via* a self-assembly method. Reproduced from ref. 161 with permission from Science China Press and Springer-Verlag GmbH Germany, part of Springer Nature, © 2021. (b) NiCo/MXene hybrid and NiCo/MXene/CNT film. Reproduced from ref. 164 with permission from the Royal Society of Chemistry, © 2021.

He *et al.*[172] reported that the dielectric parameters ε' and ε'' of $Ti_3C_2T_x$/wax composites increased as the mass fraction of $Ti_3C_2T_x$ increased. Meanwhile, both ε' and ε'' decrease with increasing EMW frequency, particularly in high-concentration (80 wt%) composites, owing to the reduced polarization capability of the absorber. The behavior of tan δ is similar to that of ε'', which indicates that conductivity and polarization have a synergistic effect on ε'' and tan δ,[172] (Fig. 10b1–b3).

In conductive polymer composites, ε' and ε'' tend to be close to zero, and the relative permeability is close to one.[173] According to eqn (1)–(3), neither complex permittivity nor relative permeability directly contributes to SE$_T$, SE$_A$, or SE$_R$. To improve the permeability, the addition of magnetic material is important. Li *et al.*[174] measured the complex permittivity and relative permeability of $Ti_3C_2T_x$/$Ni_{0.5}Zn_{0.5}Fe_2O_4$ composites in the frequency range of 0.2 to 18 GHz and found that ε' and ε'' increased as the content of conductive filler ($Ti_3C_2T_x$) increased.
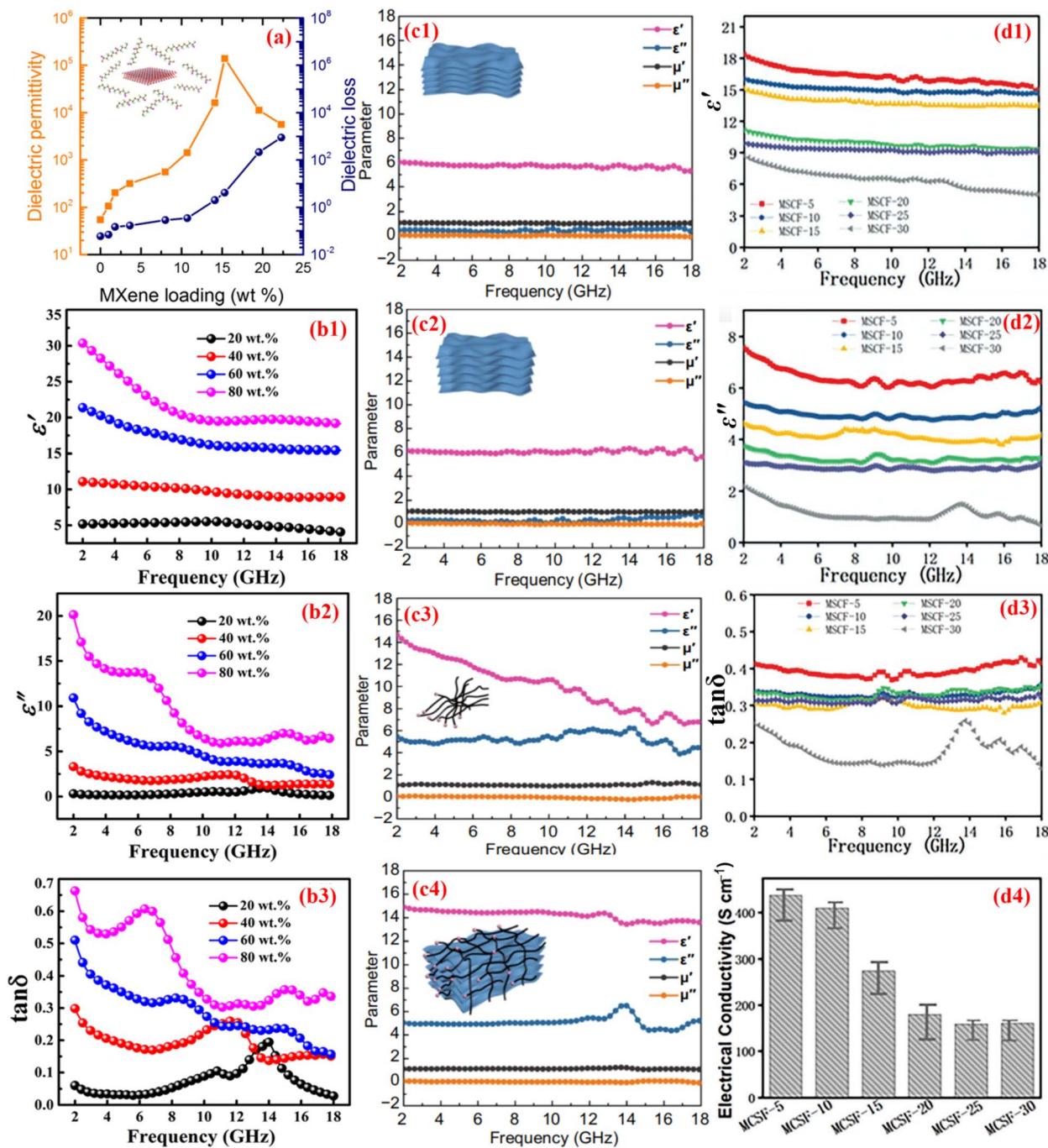
Fig. 10 Electromagnetic parameters of MXene/polymer composites. (a) Dependence of the permittivity and dielectric loss of MXene/P(VDF-TrFE-CFE) composites on the MXene content. Reproduced from ref. 170 with permission from the American Chemical Society, © 2018. (b1–b3) Dielectric parameters Ti$_3$C$_2$T$_x$/wax composites as a function of the Ti$_3$C$_2$T$_x$ mass fraction: (b1) real (ε') and (b2) imaginary (ε'') parts of complex permittivity and (b3) dielectric loss tangent (tan δ_ε). Reproduced from ref. 172 with permission from the American Chemical Society, © 2019. (c1) ε', (c2) ε'', (c3) tan δ_ε, and (c4) electrical conductibility of MCSF-5, MCSF-10, MCSF-15, MCSF-20, MCSF-25, and MCSF-30 containing 5, 10, 15, 20, 25, and 30 mg SrFe$_{12}$O$_{19}$ in the Ti$_3$C$_2$T$_x$ MXene/MWCNTs/SrFe$_{12}$O$_{19}$ film (MCSF). Reproduced from ref. 175 with permission from The Authors, © 2021. Permittivity and permeability *versus* frequency of (d1) MXene, (d2) MXene heated at 800 °C for 2 h in a N$_2$ atmosphere, (d3) CNT/Ni composite, and (d4) MXene-CNT/Ni composite. Reproduced from ref. 11 with permission from Wiley-VCH GmbH, © 2018.

However, the permeability and magnetic losses were derived from the magnetic component (Ni$_{0.5}$Zn$_{0.5}$Fe$_2$O$_4$).

Li *et al.*[175] studied the effects of Ni-based magnetic fillers on the EMI-shielding performance of MXene composites and concluded that Ni-based fillers significantly improved the complex permeability (Fig. 10c1–c4). After thermal treatment (heating at 800 °C for 2 h under a N$_2$ atmosphere), MXenes were unable to produce magnetic losses due to their inherent

dielectric properties.[176] In comparison, Ni-based samples showed a significant improvement in complex permeability.

Conductive composites with large-area junctions, such as those containing CNTs, can improve magnetic balancing and maximize the effective use of Ni nanoparticles. Huang *et al.*[11] reported that for the $Ti_3C_2T_x$-MXene/MWCNTs/SrFe$_{12}$O$_{19}$ composite film, both the complex permittivity and dielectric loss tangent (tan δ_ε) decreased as the mass fraction of magnetic plates increased, which was consistent with the trend of conductivity (Fig. 10d1–d4). However, in magnetically doped conductive composite materials, electrical and magnetic separation play crucial roles in enhancing the conductivity and maintaining efficient shielding.[177] Zhang *et al.*[178] confirmed that nanoparticle size also has a significant effect on the permittivity of EMW absorption and EMI shielding owing to relaxation and conductive losses. However, the EMW attenuation capability is determined not only by dielectric and magnetic losses[179] but also by impedance matching.[180]

Impedance matching for absorption-dominated EMI shielding in MXene/polymer composites

The impedance matching ratio plays a crucial role in the EMW absorption performance of EMI-shielding materials.[181] The impedance matching ratio Z_r, calculated using eqn (12),[182] measures the level of impedance matching between the input impedance (Z_{in}) and impedance of free space (Z_0).

$$Z_r = \left| \frac{Z_{in}}{Z_0} \right| = \left| \sqrt{\mu_r/\varepsilon_r} \tanh\left[j(2\pi ft/c)\sqrt{\mu_r\varepsilon_r} \right] \right| \quad (12)$$

where f, t, and c are the frequency of the EMW, the thickness of the sample, and the speed of light, respectively. When Z_r is close to one, EMWs are totally absorbed with minimal reflection losses.[183] However, high dielectric or magnetic losses themselves cannot guarantee high EMW absorption capacity; instead, the EMW absorption capacity is dependent on good impedance matching between the dielectric and magnetic losses.[184]

Good impedance matching is crucial for effectively absorbing incident EMWs.[175] To achieve absorption-dominated EMI shielding, the input impedance of the material should be close to that of free space (Z_0).[66] This has been confirmed by various studies, including that of Xiang *et al.*,[179] who reported an EMI SE of 110.1 dB for $Ti_3C_2T_x$/CNT/Co-nanoparticle nanocomposites. This excellent result was attributed to multiple internal reflections, electric/magnetic dipole polarization, interfacial polarization, and natural resonance loss. Multilayer structures composed of different fillers and substrates offer to facilitate fabrication and versatile design. Moreover, they can achieve excellent impedance matching and attenuation capabilities, leading to advanced EMW absorption performance. The strong EMW attenuation results from the synergistic effects of dielectric losses, magnetic losses, interfacial polarization, and impedance matching. Deng. *et al.*[185] synthesized 2D magnetized MXene composites by electrostatic assembly of negatively charged few-layered $Ti_3C_2T_x$ MXenes with positively charged hollow Fe_3O_4 nanoparticles. The MXene/hollow Fe_3O_4 hybrids

achieved a high EMW absorption performance (minimum reflection loss of 63.7 dB at a thickness of just 1.56 mm). Similar methods have also been used by Liang *et al.*[164] to optimize impedance matching and achieve efficient EMI shielding.

The ideal design of absorption-dominated MXene/polymer EMI-shielding composites comprises an asymmetric layered structure of absorption, lossy, and reflection layers, as depicted in Fig. 11. This provides a synergistic balance of dielectric losses, magnetic losses, conductivity, and impedance matching.[184] To maximize the absorption of incident EMWs, the impedance matching ratio Z_r is crucial. The closer Z_{r-1} of the absorbing layer is to one, the greater the input EM energy that can be propagated in the absorbing matrix and effectively attenuated.[44] Impedance matching between the absorption layer and free space should be maximized while minimizing the conductivity of the absorption layer (σ_1) and maximizing its permeability (μ_1).[70,186] In the lossy layer, the EMWs undergo repeated reflection and loss, which requires a medium impedance matching ratio (Z_{r-2}) and sufficient material thickness to ensure that the EMW passing through the absorption layer is exhausted. In addition, medium conductivity (σ_2) and permeability (μ_2) are suitable for the lossy layer. The loss of EMWs occurs by dielectric losses (conduction, interfacial polarization, and dipole polarization losses) and magnetic losses (magnetic resonance, magnetic coupling, and eddy current losses). To maximize the dielectric losses, a complete conductive network is required. Homogeneous, layered, porous, segregated, hybrid, and magnetic/conductive composites with complete conductive networks are favorable for EMI shielding. To minimize the transmission of EMWs through the shielding material, the impedance matching ratio (Z_{r-3}) of the reflection layer should be minimized, with an ideal reflector having a Z_{r-3} of zero. The reflection layer also requires outstanding conductivity (σ_3) and low permeability (μ_3).[187] Thus, the conductivity, impedance matching ratio, and permeability of the absorbing, lossy, and reflective layers of an ideal absorption-dominated shielding material with an asymmetric layered structure should have gradients in the order $\sigma_1 < \sigma_2 < \sigma_3$, $Z_{r-1} > Z_{r-2} > Z_{r-3}$, and $\mu_1 > \mu_2 > \mu_3$, respectively.

Ji *et al.*[186] utilized this concept to design a multilayer MXene/polymer composite with an impedance gradient that exhibits absorption-dominated EMI-shielding behavior. The composite
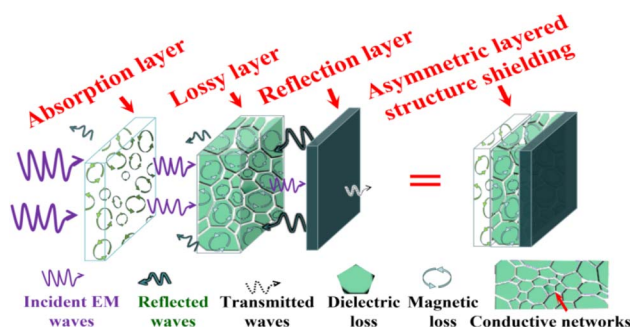

Fig. 11 Ideal absorption-dominated shield model of an asymmetric layered structure.

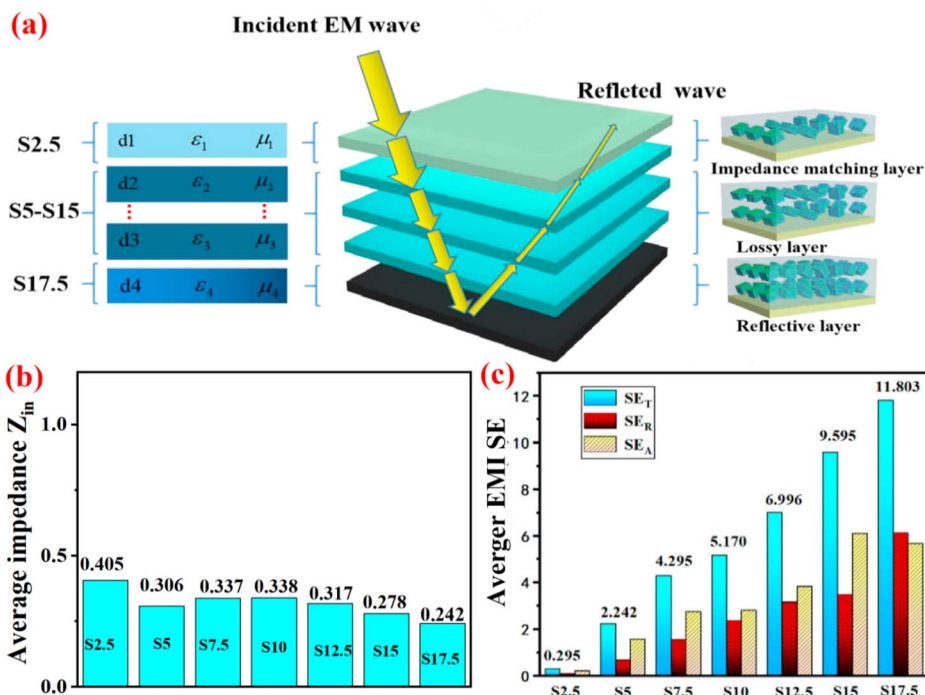© 2023 The Author(s). Published by the Royal Society of Chemistry

Fig. 12   (a) Multilayer impedance gradient structure consisting of $Ti_3C_2T_x$ MXene/polymer films; (b) the average impedance Z_{in} of S2.5–S17.5; (c) the average sEMI SE of the samples S2.5–S17.5. Reproduced from ref. 186 with permission from Elsevier Ltd., © 2021.

was fabricated from laminated cast films by a lamination approach, affording multilayer samples S2.5 (the $Ti_3C_2T_x$ content is 2.5 wt%), S5–S15, and S17.5, as shown in Fig. 12a.

The low permittivity of S2.5 and the well-matched impedance used as the top surface layer ensure that the incident EMW enters the specimen rather than being reflected off the surface. The dielectric film of S5–S15 has moderate permittivity and strong dielectric loss capability and can be used as an EMW-absorbing layer. The efficiency of converting the EM energy into heat is enhanced and the effective absorption of the EMWs. A high SE_R value resulted in repeated EMW losses in S5–S15. This significantly improves the attenuation of EMWs by the multilayer impedance gradient composite film. Notably, the composite film had a gradual impedance gradient ranging from excellent impedance matching ($Z_r = 0.405$) to impedance mismatching ($Z_r = 0.242$), which ensured that the incident EMWs entered the sample without reflecting from the surface, as shown in Fig. 12b. The dielectric losses were also gradated from weak to strong. This multilayer impedance gradient design integrates various loss mechanisms such as conduction, dielectric loss, and reflection, resulting in an excellent EMI SE of 11.8 dB at 15 wt% $Ti_3C_2T_x$ MXene and a thickness of only 0.1 mm (Fig. 12c). The average SE_T, SE_R, and SE_A values for the top and bottom sections of the composite film for the various test orientations are 11.82 and 11.82 dB, 7.87 and 8.09 dB, 3.95 and 3.73 dB, respectively. However, further investigation is required to determine if the subtle changes in the EMI shielding performance during the test sequence are a result of the dissipation of the majority of EMWs in the lossy layer and the inability of the reflection layer to perform its function. Xing

et al.[188] also fabricated an ultrathin asymmetric layered MXene@AgNW@MoS_2 composite film (with a thickness of 0.03 mm) comprising five alternating internal layers and MoS_2 outer layers by atomic layer deposition. This ultrathin asymmetric layered structure effectively increased the absorption proportion of EMWs, reduced the secondary reflection, and improved the stability of EMI shielding properties, achieving an excellent EMI SE of 86.3 dB in the X-band.

Our previous research[189] confirmed the importance of optimized impedance matching for absorption-dominated efficient EMI shielding of MXene/polymer composites. The above comparisons show that MXene/polymer composites with different Z_r values exhibit different EMI SE. MXene/polymer composites with better matched Z_r (0.20–0.27) and high conductivity exhibited a high EMI SE of 46.1 dB with an absorption coefficient of 85.7%. Therefore, rational design with appropriate impedance matching is crucial for achieving absorption-dominated EMI shielding in MXene/polymer composites.

Conclusion and outlook

Excellent conductive filler networks and structural design play key roles in the outstanding absorption-dominated green EMI shielding performance of MXene/polymer composites. Homogeneous, layered, porous, and segregated composite structures are capable of enhancing internal scattering for EMI shielding, while hybrid and magnetic/conducting structures overcome the shortcomings of individual structural designs, enabling the full exploitation of the advantages of structural features to improve EMI SE. However, combining multiple structural designs adds

complexity and processing cost. Indeed, the complete conductance network for electromagnetic separation and the design of appropriate impedance matching favor the absorption-dominated EMI shielding of MXene/polymer composites. To improve the absorption-dominated EMI shielding of MXene/polymer composites, the following points should be considered:

(1) The MXene preparation process should use mild reaction conditions to preserve the high conductivity and 2D flake morphology of MXenes in polymer composites. The assembly method of MXenes should also be improved to ensure their uniform distribution and orientation.

(2) The conductive network in MXene/polymer composites with hybrid and magnetic/conducting structures should be intact and continuous to achieve excellent impedance matching and enhance magnetic losses. The combination of dielectric and magnetic losses can result in efficient absorption-dominated green EMI shielding.

(3) Structural and functional design techniques should be integrated to reduce the MXene content in the composites. The structure and impedance matching of the MXene/polymer composite should be carefully chosen to favor absorption-dominated green EMI shielding. This review provides theoretical guidance for practical solutions to reduce EMI pollution.

(4) Heterostructures have strong interfacial polarization capability, which can improve the EMW loss performance of MXene/polymer materials. However, the toughness of heterostructured composites is negatively affected by interfacial stress. Thus, a processing strategy that imparts good mechanical strength is necessary to enhance the overall mechanical properties of the composite for practical applications.

Green absorption EMI shielding is an emerging and promising technique that can address the challenges of EMW pollution in modern military and civilian applications. It can achieve both high EMI shielding performance and energy conversion efficiency by optimizing the material composition and structure. More research is needed to explore the design principles and fabrication methods of green absorption EMI shielding materials, as well as their potential applications in various fields. According to a recent perspective,[190] a new generation of energy harvesting MXene/polymer composite electromagnetic materials is emerging.

Author contributions

Qimei Zhang: investigation, original draft. Qi Wang: editing, visualization. Jian Cui: resources, funding acquisition. Shuai Zhao: formal analysis. Ailin Gao: investigation. Guangfa Zhang: editing. Yehai Yan: conceptualization and project administration.

Conflicts of interest

There are no conflicts to declare.

Acknowledgements

Notes and references

1 J. Kruželák, A. Kvasničáková, K. Hložeková and I. Hudec, *Nanoscale Adv.*, 2021, **3**, 123–172.

2 C. Wang, V. Murugadoss, J. Kong, Z. He, X. Mai, Q. Shao, Y. Chen, L. Guo, C. Liu and S. Angaiah, *Carbon*, 2018, **140**, 696–733.

3 J. Cheng, C. Li, Y. Xiong, H. Zhang, H. Raza, S. Ullah, J. Wu, G. Zheng, Q. Cao and D. Zhang, *Nano-Micro Lett.*, 2022, **14**, 80.

4 S. Schelkunoff, *Electromagnetic waves*, ed. Van Nostrand, New York, 1943.

5 M. Vural, A. Pena-Francesch, J. Bars-Pomes, H. Jung, H. Gudapati, C. B. Hatter, B. D. Allen, B. Anasori, I. T. Ozbolat and Y. Gogotsi, *Adv. Funct. Mater.*, 2018, **28**, 1801972.

6 L. Liang, P. Xu, Y. Wang, Y. Shang, J. Ma, F. Su, Y. Feng, C. He, Y. Wang and C. Liu, *Chem. Eng. J.*, 2020, **395**, 125209.

7 Y. Yang, B. Li, N. Wu, W. Liu, S. Zhao, C. J. Zhang, J. Liu and Z. Zeng, *ACS Mater. Lett.*, 2022, **4**, 2352–2361.

8 D. X. Yan, H. Pang, B. Li, R. Vajtai, L. Xu, P. G. Ren, J. H. Wang and Z. M. Li, *Adv. Funct. Mater.*, 2015, **25**, 559–566.

9 Y. Zhan, M. Oliviero, J. Wang, A. Sorrentino, G. G. Buonocore, L. Sorrentino, M. Lavorgna, H. Xia and S. Iannace, *Nanoscale*, 2019, **11**, 1011–1020.

10 Y. Zhan, J. Wang, K. Zhang, Y. Li, Y. Meng, N. Yan, W. Wei, F. Peng and H. Xia, *Chem. Eng. J.*, 2018, **344**, 184–193.

11 M. Huang, L. Wang, X. Li, Z. Wu, B. Zhao, K. Pei, X. Liu, X. Zhang and R. Che, *Small*, 2022, **18**, 2201587.

12 J. Yin, J. Zhang, S. Zhang, C. Liu, X. Yu, L. Chen, Y. Song, S. Han, M. Xi and C. Zhang, *Chem. Eng. J.*, 2021, **421**, 129763.

13 C. Han, H. Zhang, D. Zhang, Y. Deng, J. Shen and G. Zeng, *Nanomaterials*, 2020, **10**, 598.

14 R. Peymanfar, E. Selseleh-Zakerin, A. Ahmadi and S. H. Tavassoli, *Sci. Rep.*, 2021, **11**, 11932.

15 R. Peymanfar, S. Javanshir, M. R. Naimi-Jamal and S. H. Tavassoli, *J. Mater. Sci.*, 2021, **56**, 17457–17477.

16 P. Liu, V. M. H. Ng, Z. Yao, J. Zhou and L. B. Kong, *Mater. Lett.*, 2018, **229**, 286–289.

17 T. Koschny, M. Kafesaki, E. Economou and C. Soukoulis, *Phys. Rev. Lett.*, 2004, **93**, 107402.

18 Y. Qiao, X. Liu, B. Li, Y. Han, Y. Zheng, K. W. K. Yeung, C. Li, Z. Cui, Y. Liang and Z. Li, *Nat. Commu.*, 2020, **11**, 4446.

19 A. Chaudhary, S. Kumari, R. Kumar, S. Teotia, B. P. Singh, A. P. Singh, S. Dhawan and S. R. Dhakate, *ACS Appl. Mater. Interfaces*, 2016, **8**, 10600–10608.

20 S. Geetha, K. Satheesh Kumar, C. R. Rao, M. Vijayan and D. Trivedi, *J. Appl. Polym. Sci.*, 2009, **112**, 2073–2086.

21 A. N. Esfahani, A. Katbab, A. Taeb, L. Simon and M. A. Pope, *Eur. Polym. J.*, 2017, **95**, 520–538.

22 B. Shen, Y. Li, W. Zhai and W. Zheng, *ACS Appl. Mater. Interfaces*, 2016, **8**, 8050–8057.

23 J. M. Thomassin, C. Jerome, T. Pardoen, C. Bailly, I. Huynen and C. Detrembleur, *Mater. Sci. Eng., R*, 2013, **74**, 211–232.

24 Y. Fei, M. Liang, T. Zhou, Y. Chen and H. Zou, *Carbon*, 2020, **167**, 575–584.

25 S. A. Schelkunoff, *Proc. IRE*, 1937, **25**, 1457–1492.

26 S. Liu, S. Qin, Y. Jiang, P. Song and H. Wang, *Composites, Part A*, 2021, **145**, 106376.

27 X. H. Li, X. Li, K. N. Liao, P. Min, T. Liu, A. Dasari and Z. Z. Yu, *ACS Appl. Mater. Interfaces*, 2016, **8**, 33230–33239.

28 M. Verma, A. P. Singh, P. Sambyal, B. P. Singh, S. Dhawan and V. Choudhary, *Phys. Chem. Chem. Phys.*, 2015, **17**, 1610–1618.

29 D. Chung and A. A. Eddib, *Carbon*, 2019, **141**, 685–691.

30 Y. Tao, P. Li and S. Q. Shi, *Materials*, 2016, **9**, 540.

31 C. R. Paul, *Introduction to Electromagnetic Compatibility*, John Wiley and Sons, Inc., Hoboken, NJ, USA, 2006.

32 X. Liu, X. Yin, L. Kong, Q. Li, Y. Liu, W. Duan, L. Zhang and L. Cheng, *Carbon*, 2014, **68**, 501–510.

33 G. M. Kunke, *Shielding of Electromagnetic Waves*, Springer, Cham, Switzerland, 2020.

34 J. Wojkiewicz, S. Fauveaux, N. Redon and J. Miane, *Int. J. Electron.*, 2004, **19**, 203–206.

35 M. Yuan, Y. Fei, H. Zhang, B. Qiu, L. Shen, X. He, M. Liang, S. Zhou, Y. Chen and H. Zou, *Composites, Part B*, 2022, **233**, 109622.

36 H. Bizhani, V. Nayyeri, A. Katbab, A. Jalali-Arani and H. Nazockdast, *Eur. Polym. J.*, 2018, **100**, 209–218.

37 F. Shahzad, M. Alhabeb, C. B. Hatter, B. Anasori, S. Man Hong, C. M. Koo and Y. Gogotsi, *Science*, 2016, **353**, 1137–1140.

38 A. Iqbal, P. Sambyal and C. M. Koo, *Adv. Funct. Mater.*, 2020, **30**, 2000883.

39 L. Zhang, N. T. Alvarez, M. Zhang, M. Haase, R. Malik, D. Mast and V. Shanov, *Carbon*, 2015, **82**, 353–359.

40 G. Lovat, P. Burghignoli, R. Araneo, E. Stracqualursi and S. Celozzi, *IEEE Trans. Electromagn. Compat.*, 2020, **63**, 631–635.

41 R. Kumar, A. Sharma, A. Pandey, A. Chaudhary, N. Dwivedi, M. M. Shafeeq, D. Mondal and A. Srivastava, *Sci. Rep.*, 2020, **10**, 9913.

42 M. H. Al-Saleh, W. H. Saadeh and U. Sundararaj, *Carbon*, 2013, **60**, 146–156.

43 P. Song, B. Liu, H. Qiu, X. Shi, D. Cao and J. Gu, *Compos. Commun.*, 2021, **24**, 100653.

44 Y. He, Y. Shao, Y. Xiao, J. Yang, X. Qi and Y. Wang, *ACS Appl. Mater. Interfaces*, 2022, **14**, 6057–6070.

45 S. Zhang, Y. Wang, Q. Ran, Q. Fu and Y. Gu, *React. Funct. Polym.*, 2019, **143**, 104324.

46 X. Yang, S. Fan, Y. Li, Y. Guo, Y. Li, K. Ruan, S. Zhang, J. Zhang, J. Kong and J. Gu, *Composites, Part A*, 2020, **128**, 105670.

47 H. Jia, Z. L. Yi, X. H. Huang, F. Y. Su, Q. Q. Kong, X. Yang, Z. Wang, L. J. Xie, Q. G. Guo and C. M. Chen, *Carbon*, 2021, **183**, 809–819.

48 X. Li, W. You, L. Wang, J. Liu, Z. Wu, K. Pei, Y. Li and R. Che, *ACS Appl. Mater. Interfaces*, 2019, **11**, 44536–44544.

49 B. Shen, W. Zhai, M. Tao, J. Ling and W. Zheng, *ACS Appl. Mater. Interfaces*, 2013, **5**, 11383–11391.

50 J. C. Lei, X. Zhang and Z. Zhou, *Front. Phys.*, 2015, **10**, 276–286.

51 M. Naguib, M. Kurtoglu, V. Presser, J. Lu, J. Niu, H. Min, L. Hultman, Y. Gogotsi and M. W. Barsoum, *Adv. Mater.*, 2011, **23**, 4248–4253.

52 M. Ghidiu, M. R. Lukatskaya, M. Q. Zhao, Y. Gogotsi and M. W. Barsoum, *Nature*, 2014, **516**, 78–81.

53 Y. Li, H. Shao, Z. Lin, J. Lu, L. Liu, B. Duployer, P. O. Persson, P. Eklund, L. Hultman and M. Li, *Nat. Mater.*, 2020, **19**, 894–899.

54 D. Xiong, X. Li, Z. Bai and S. Lu, *Small*, 2018, **14**, 1703419.

55 L. Wang, M. Zhang, B. Yang, J. Tan and X. Ding, *ACS Nano*, 2020, **14**, 10633–10647.

56 J. V. Vaghasiya, C. C. Mayorga-Martinez, J. Vyskoil, Z. Sofer and M. Pumera, *Adv. Funct. Mater.*, 2020, **30**, 2003673.

57 V. Kamysbayev, A. S. Filatov, H. Hu, X. Rui, F. Lagunas, D. Wang, R. F. Klie and D. V. Talapin, *Science*, 2020, **369**, 979–983.

58 C. J. Zhang, S. Pinilla, N. Mcevoy, C. P. Cullen, B. Anasori, E. Long, S. H. Park, A. Seralascaso, A. Shmeliov and D. Krishnan, *Chem. Mater.*, 2017, **29**, 4848–4856.

59 Y. Y. Peng, B. Akuzum, N. Kurra, M. Q. Zhao, M. Alhabeb, B. Anasori, E. C. Kumbur, H. N. Alshareef, M. D. Ger and Y. Gogotsi, *Energy Environ. Sci.*, 2016, **9**, 2847–2854.

60 S. Zhang, H. Ying, B. Yuan, R. Hu and W. Q. Han, *Nano-Micro Lett.*, 2020, **12**, 78.

61 S. Wan, X. Li, Y. Chen, N. Liu, S. Wang, Y. Du, Z. Xu, X. Deng, S. Dou, L. Jiang and Q. Cheng, *Nat. Commun.*, 2022, **13**, 7340.

62 T. Yun, H. Kim, A. Iqbal, Y. S. Cho, G. S. Lee, M. K. Kim, S. J. Kim, D. Kim, Y. Gogotsi and S. O. Kim, *Adv. Mater.*, 2020, **32**, 1906769.

63 M. Han, C. E. Shuck, R. Rakhmanov, D. Parchment, B. Anasori, C. M. Koo, G. Friedman and Y. Gogotsi, *ACS Nano*, 2020, **14**, 5008–5016.

64 Y. Zhang, Y. Yan, H. Qiu, Z. Ma, K. Ruan and J. Gu, *J. Mater. Sci. Technol.*, 2022, **103**, 42–49.

65 C. Liang, Z. Gu, Y. Zhang, Z. Ma, H. Qiu and J. Gu, *Nano-Micro Lett.*, 2021, **13**, 181.

66 S. Li, X. Tang, Y. Zhang, Q. Lan, Z. Hu, L. Li, N. Zhang, P. Ma, W. Dong and W. Tjiu, *ACS Appl. Mater. Interfaces*, 2022, **14**, 8297–8310.

67 Y. Li, B. Shen, D. Yi, L. Zhang, W. Zhai, X. Wei and W. Zheng, *Compos. Sci. Technol.*, 2017, **138**, 209–216.

68 X. Su, J. Wang, X. Zhang, B. Zhang, Q. Wu, W. Dai, Y. Zou and C. Shao, *Mater. Lett.*, 2019, **239**, 136–139.

69 L. Liang, Q. Li, X. Yan, Y. Feng, Y. Wang, H. B. Zhang, X. Zhou, C. Liu, C. Shen and X. Xie, *ACS Nano*, 2021, **15**, 6622–6632.

70 J. M. Thomassin, C. Pagnoulle, L. Bednarz, I. Huynen, R. Jerome and C. Detrembleur, *J. Mater. Chem.*, 2008, **18**, 792–796.

71 Q. Hu, X. Qi, H. Cai, R. Xie, L. Long, Z. Bai, Y. Jiang, S. Qin, W. Zhong and Y. Du, *Sci. Rep.*, 2017, **7**, 11213.

72 H. Pang, L. Xu, D. X. Yan and Z. M. Li, *Prog. Polym. Sci.*, 2014, **39**, 1908–1933.

73 K. Rajavel, S. Luo, Y. Wan, X. Yu and C. Wong, *Composites, Part A*, 2019, **129**, 105693.

74 L. Wang, L. Chen, P. Song, C. Liang, Y. Lu, H. Qiu, Y. Zhang, J. Kong and J. Gu, *Composites, Part B*, 2019, **171**, 111–118.

75 J. Liu, L. Mckeon, J. Garcia, S. Pinilla, S. Barwich, M. Möbius, P. Stamenov, J. N. Coleman and V. Nicolosi, *Adv. Mater.*, 2022, **34**, 2106253.

76 Y. Dai, X. Wu, L. Li, Y. Zhang, Z. Deng, Z. Z. Yu and H. B. Zhang, *J. Mater. Chem. A*, 2022, **10**, 11375–11385.

77 T. B. Ma, H. Ma, K. P. Ruan, X. T. Shi, H. Qiu, S. Y. Gao and J. W. Gu, *Chin. J. Polym. Sci.*, 2022, **40**, 248–255.

78 Y. Zhang, K. Ruan and J. Gu, *Small*, 2021, **17**, 2101951.

79 S. Jayaraman, T. J. Rawson and M. A. Belyustina, *Energy Environ. Sci.*, 2022, **15**, 2948–2957.

80 L. Q. Zhang, B. Yang, J. Teng, J. Lei, D. X. Yan, G. J. Zhong and Z. M. Li, *J. Mater. Chem. C*, 2017, **5**, 3130–3138.

81 Z. Ma, S. Kang, J. Ma, L. Shao, Y. Zhang, C. Liu, A. Wei, X. Xiang, L. Wei and J. Gu, *ACS Nano*, 2020, **14**, 8368–8382.

82 H. Wei, M. Wang, W. Zheng, Z. Jiang and Y. Huang, *Ceram. Int.*, 2020, **46**, 6199–6204.

83 Z. Liu, W. Wang, J. Tan, J. Liu, M. Zhu, B. Zhu and Q. Zhang, *J. Mater. Chem. C*, 2020, **8**, 7170–7180.

84 B. Zhou, Z. Zhang, Y. Li, G. Han, Y. Feng, B. Wang, D. Zhang, J. Ma and C. Liu, *ACS Appl. Mater. Interfaces*, 2020, **12**, 4895–4905.

85 Y. Zhang, W. Cheng, W. Tian, J. Lu and Y. Hu, *ACS Appl. Mater. Interfaces*, 2020, **12**, 6371–6382.

86 X. Jin, J. Wang, L. Dai, X. Liu, L. Li, Y. Yang, Y. Cao, W. Wang, H. Wu and S. Guo, *Chem. Eng. J.*, 2020, **380**, 122475.

87 C. Lei, Y. Zhang, D. Liu, K. Wu and Q. Fu, *ACS Appl. Mater. Interfaces*, 2020, **12**, 26485–26495.

88 R. Liu, M. Miao, Y. Li, J. Zhang, S. Cao and X. Feng, *ACS Appl. Mater. Interfaces*, 2018, **10**, 44787–44795.

89 J. Q. Luo, S. Zhao, H. B. Zhang, Z. Deng, L. Li and Z. Z. Yu, *Compos. Sci. Technol.*, 2019, **182**, 107754.

90 Y. Zhang, Z. Ma, K. Ruan and J. Gu, *Research*, 2022, **2**, 213–224.

91 S. Habibpour, K. Zarshenas, M. Zhang, M. Hamidinejad, L. Ma, C. B. Park and A. Yu, *ACS Appl. Mater. Interfaces*, 2022, **14**, 21521–21534.

92 G. M. Weng, J. Li, M. Alhabeb, C. Karpovich, H. Wang, J. Lipton, K. Maleski, J. Kong, E. Shaulsky and M. Elimelech, *Adv. Funct. Mater.*, 2018, **28**, 1803361.

93 B. Zhou, M. Yang, D. Han, G. Feng, Y. Wang, B. Ma, J. Ma, J. Ma, C. Liu and C. Shen, *ACS Appl. Mater. Interfaces*, 2020, **12**, 40859–40869.

94 W. Chen, L. X. Liu, H. B. Zhang and Z. Z. Yu, *ACS Nano*, 2020, **14**, 16643–16653.

95 X. Jin, J. Wang, L. Dai, X. Liu, L. Li, Y. Yang, Y. Cao, W. Wang, H. Wu and S. Guo, *Chem. Eng. J.*, 2020, **380**, 122475.

96 M. Ying, R. Zhao, X. Hu, Z. Zhang, W. Liu, J. Yu, X. Liu, X. Liu, H. Rong and C. Wu, *Angew. Chem.*, 2022, **134**, e202201323.

97 Y. Wang, H. K. Peng, T. T. Li, B. C. Shiu, H. T. Ren, X. Zhang, C. W. Lou and J. H. Lin, *Chem. Eng. J.*, 2021, **412**, 128681.

98 W. T. Cao, F. F. Chen, Y. J. Zhu, Y. G. Zhang and F. Chen, *ACS Nano*, 2018, **12**, 4583–4593.

99 X. Liu, X. Jin, L. Li, J. Wang and W. Wang, *J. Mater. Chem. A*, 2020, **8**, 12526–12537.

100 Q. W. Wang, H. B. Zhang, J. Liu, S. Zhao, X. Xie, L. Liu, R. Yang, N. Koratkar and Z. Z. Yu, *Adv. Funct. Mater.*, 2019, **29**, 1806819.

101 L. Geng, P. Zhu, Y. Wei, R. Guo, C. Xiang, C. Cui and Y. Li, *Cellulose*, 2019, **26**, 2833–2847.

102 D. Y. Li, L. X. Liu, Q. W. Wang, H. B. Zhang, W. Chen, G. Yin and Z. Z. Yu, *ACS Appl. Mater. Interfaces*, 2022, **14**, 12703–12712.

103 C. Lan, H. Jia, M. Qiu and S. Fu, *ACS Appl. Mater. Interfaces*, 2021, **13**, 38761–38772.

104 Y. Guo, H. Qiu, K. Ruan, Y. Zhang and J. Gu, *Nano-Micro Lett.*, 2022, **14**, 26.

105 W. Cao, C. Ma, S. Tan, M. Ma and F. Chen, *Nano-Micro Lett.*, 2019, **11**, 1–17.

106 J. Zhang, J. Li, G. Tan, R. Hu, J. Wang, C. Chang and X. Wang, *ACS Appl. Mater. Interfaces*, 2017, **9**, 42192–42199.

107 Z. Lei, D. Tian, X. Liu, J. Wei, K. Rajavel, T. Zhao, Y. Hu, P. Zhu, R. Sun and C. P. Wong, *Chem. Eng. J.*, 2021, **424**, 130365.

108 Y. Cheng, X. Li, Y. Qin, Y. Fang, G. Liu, Z. Wang, J. Matz, P. Dong, J. Shen and M. Ye, *Sci. Adv.*, 2021, **7**, eabj1663.

109 C. Liang, Y. Liu, Y. Ruan, H. Qiu, P. Song, J. Kong, H. Zhang and J. Gu, *Composites, Part A*, 2020, **139**, 106143.

110 W. Tian, A. VahidMohammadi, Z. Wang, L. Ouyang, M. Beidaghi and M. M. Hamedi, *Nat. Commun.*, 2019, **10**, 2558.

111 T. Kuang, L. Chang, F. Chen, Y. Sheng, D. Fu and X. Peng, *Carbon*, 2016, **105**, 305–313.

112 F. Bu, M. M. Zagho, Y. Ibrahim, B. Ma, A. Elzatahry and D. Zhao, *Nano Today*, 2020, **30**, 100803.

113 Y. Yao, S. Jin, H. Zou, L. Li, X. Ma, G. Lv, F. Gao, X. Lv and Q. Shu, *J. Mater. Sci.*, 2021, **56**, 6549–6580.

114 R. Bian, G. He, W. Zhi, S. Xiang, T. Wang and D. Cai, *J. Mater. Chem. C*, 2019, **7**, 474–478.

115 Y. Wang, J. Yang, Z. Chen and Y. Hu, *RSC Adv.*, 2019, **9**, 41038–41049.

116 J. Liu, H. B. Zhang, R. Sun, Y. Liu, Z. Liu, A. Zhou and Z. Z. Yu, *Adv. Mater.*, 2017, **29**, 1702367.

117 X. Li, X. Yin, C. Song, M. Han, H. Xu, W. Duan, L. Cheng and L. Zhang, *Adv. Funct. Mater.*, 2018, **28**, 1803938.

118 Z. Deng, P. Tang, X. Wu, H. Zhang and Z. Yu, *ACS Appl. Mater. Interfaces*, 2021, **13**, 20539–20547.

119 M. S. Cao, Y. Z. Cai, P. He, J. C. Shu, W. Q. Cao and J. Yuan, *Chem. Eng. J.*, 2019, **359**, 1265–1302.

120 Q. Wang, J. Zhang, Z. Zhang, Y. Hao and K. Bi, *Adv. Compos. Hybrid Mater.*, 2020, **3**, 58–65.

121 T. Zhou, C. Zhao, Y. Liu, J. Huang, H. Zhou, Z. Nie, M. Fan, T. Zhao, Q. Cheng and M. Liu, *ACS Nano*, 2022, **16**, 12013–12023.

122 A. P. P. Fugolin, A. R. Costa, L. Correr-Sobrinho, R. Crystal Chaw, S. Lewis, J. L. Ferracane and C. S. Pfeifer, *Sci. Rep.*, 2021, **11**, 7638.

123 R. Sun, H. B. Zhang, J. Liu, X. Xie, R. Yang, Y. Li, S. Hong and Z. Z. Yu, *Adv. Funct. Mater.*, 2017, **27**, 1702807.

124 P. Song, Z. Ma, H. Qiu, Y. Ru and J. Gu, *Nano-Micro Lett.*, 2022, **14**, 51.

125 P. Song, B. Liu, C. Liang, K. Ruan, H. Qiu, Z. Ma, Y. Guo and J. Gu, *Nano-Micro Lett.*, 2021, **13**, 91.

126 S. Zhao, H. B. Zhang, J. Q. Luo, Q. W. Wang, B. Xu, S. Hong and Z. Z. Yu, *ACS Nano*, 2018, **12**, 11193–11202.

127 X. Wu, B. Han, H. B. Zhang, X. Xie, T. Tu, Y. Zhang, Y. Dai, R. Yang and Z. Z. Yu, *Chem. Eng. J.*, 2020, **381**, 122622.

128 L. Wang, P. Song, C. T. Lin, J. Kong and J. Gu, *Research*, 2020, **2020**, 4093732.

129 L. Wang, H. Qiu, P. Song, Y. Zhang, Y. Lu, C. Liang, J. Kong, L. Chen and J. Gu, *Composites, Part A*, 2019, **123**, 293–300.

130 Y. Zhang and J. Gu, *Nano-Micro Lett.*, 2022, **14**, 89.

131 Y. Yang, N. Wu, B. Li, W. Liu, F. Pan, Z. Zeng and J. Liu, *ACS Nano*, 2022, **16**, 15042–15052.

132 W. Ma, W. Cai, W. Chen, P. Liu, J. Wang and Z. Liu, *Chem. Eng. J.*, 2021, **426**, 130729.

133 Z. H. Zeng, N. Wu, J. J. Wei, Y. F. Yang, T. T. Wu, B. Li, S. B. Hauser, W. D. Yang, J. R. Liu and S. Y. Zhao, *Nano-Micro Lett.*, 2022, **14**, 59.

134 V. T. Nguyen, B. K. Min, Y. Yi, S. J. Kim and C. G. Choi, *Chem. Eng. J.*, 2020, **393**, 124608.

135 M. Han, X. Yin, K. Hantanasirisakul, X. Li, A. Iqbal, C. B. Hatter, B. Anasori, C. M. Koo, T. Torita and Y. Soda, *Adv. Opt. Mater.*, 2019, **7**, 1900267.

136 M. H. Al-Saleh, G. A. Gelves and U. Sundararaj, *Composites, Part A*, 2011, **42**, 92–97.

137 D. X. Yan, H. Pang, L. Xu, Y. Bao, P. G. Ren, J. Lei and Z. M. Li, *Nanotechnology*, 2014, **25**, 145705.

138 J. Q. Luo, S. Zhao, H. B. Zhang, Z. Deng, L. Li and Z. Z. Yu, *Compos. Sci. Technol.*, 2019, **182**, 107754.

139 W. Ma, W. Cai, W. Chen, P. Liu, J. Wang and Z. Liu, *Chem. Eng. J.*, 2021, **425**, 131699.

140 D. Xu, W. Chen and P. Liu, *Compos. Sci. Technol.*, 2020, **199**, 108355.

141 D. Feng, Q. Wang, D. Xu and P. Liu, *Compos. Sci. Technol.*, 2019, **182**, 107753.

142 W. C. Yu, J. Z. Xu, Z. G. Wang, Y. F. Huang, H. M. Yin, L. Xu, Y. W. Chen, D. X. Yan and Z. M. Li, *Composites, Part A*, 2018, **110**, 237–245.

143 Y. Sliozberg, J. Andzelm, C. B. Hatter, B. Anasori and A. Hall, *Compos. Sci. Technol.*, 2020, **192**, 108124.

144 J. Jimmy and B. Kandasubramanian, *Eur. Polym. J.*, 2019, **122**, 109367.

145 H. Zhang, L. Wang, C. Qiang, L. Ping and Q. Hu, *Mater. Des.*, 2016, **92**, 682–689.

146 M. Nanko, *AZojomo*, 2009, **6**, 1–8.

147 Z. Wang, G. Meng, L. Wang, L. Tian, S. Chen, G. Wu, B. Kong and Y. Cheng, *Sci. Rep.*, 2021, **11**, 2495.

148 C. Weng, G. Wang, Z. Dai, Y. Pei, L. Liu and Z. Zhang, *Nanoscale*, 2019, **11**, 22804–22812.

149 X. Jia, B. Shen, L. Zhang and W. Zheng, *Carbon*, 2021, **173**, 932–940.

150 F. Ye, Y. Zhang, C. Addiego, M. Xu, H. Huyan, X. Ren and X. Pan, *npj Comput. Mater.*, 2021, **7**, 130.

151 B. Zhao, Z. Ma, Y. Sun, Y. Han and J. Gu, *Small Struct.*, 2022, **3**, 2200162.

152 Y. Zhang, K. Ruan, K. Zhou and J. Gu, *Adv. Mater.*, 2023, **35**, 2211642.

153 X. Wang, B. Wen and X. Yang, *Composites, Part B*, 2019, **173**, 106904.

154 Y. Zhang, Z. Ma, K. Ruan and J. Gu, *Nano Res.*, 2022, **15**, 5601–5609.

155 S. Jiang, K. Qian, K. Yu, H. Zhou, Y. Weng and Z. Zhang, *Compos. Commun.*, 2020, **20**, 100363.

156 L. Wang, Q. Quan, L. Zhang, L. Cheng, P. Lin, S. Pan and Z. Zhong, *J. Magn. Magn. Mater.*, 2018, **449**, 385–389.

157 Y. Zhan, J. Wang, K. Zhang, Y. Li, Y. Meng, N. Yan, W. Wei, F. Peng and H. Xia, *Chem. Eng. J.*, 2018, **344**, 184–193.

158 K. Raagulan, R. Braveenth, L. R. Lee, J. Lee, B. M. Kim, J. J. Moon, S. B. Lee and K. Y. Chai, *Nanomaterials*, 2019, **9**, 519.

159 L. Liang, G. Han, Y. Li, B. Zhao, B. Zhou, Y. Feng, J. Ma, Y. Wang, R. Zhang and C. Liu, *ACS Appl. Mater. Interfaces*, 2019, **11**, 25399–25409.

160 S. J. Wang, D. S. Li and L. Jiang, *Adv. Mater. Interfaces*, 2019, **6**, 1900961.

161 Q. Song, B. Chen, Z. Zhou and C. Lu, *Sci. China Mater.*, 2021, **64**, 1437–1448.

162 Y. Wang, Q. Qi, G. Yin, W. Wang and D. Yu, *ACS Appl. Mater. Interfaces*, 2021, **13**, 21831–21843.

163 S. Hu, S. Li, W. Xu, W. Yu and Y. Zhou, *Ceram. Int.*, 2021, **47**, 29995–30004.

164 L. Liang, C. Yao, X. Yan, Y. Feng, X. Hao, B. Zhou, Y. Wang, J. Ma, C. Liu and C. Shen, *J. Mater. Chem. A*, 2021, **9**, 24560–24570.

165 C. Wen, X. Li, R. Zhang, C. Xu, W. You, Z. Liu, B. Zhao and R. Che, *ACS Nano*, 2022, **16**, 1150–1159.

166 M. Ma, W. Tao, X. Liao, S. Chen, Y. Shi, H. He and X. Wang, *Chem. Eng. J.*, 2023, **452**, 139471.

167 X. Li, Z. Wu, W. You, L. Yang and R. Che, *Nano-Micro Lett.*, 2022, **14**, 73.

168 T. Chen, F. Deng, J. Zhu, C. Chen, G. Sun, S. Ma and X. Yang, *J. Mater. Chem.*, 2012, **22**, 15190–15197.

169 B. Zhang, G. Tian, D. Xiong, T. Yang, F. Chun, S. Zhong, Z. Lin, W. Li and W. Yang, *Research*, 2021, **2021**, 7189376.

170 S. Tu, Q. Jiang, X. Zhang and H. N. Alshareef, *ACS Nano*, 2018, **12**, 3369–3377.

171 H. Luo, W. Feng, C. Liao, L. Deng, S. Liu, H. Zhang and P. Xiao, *J. Appl. Phys.*, 2018, **123**, 104103.

172 P. He, M. S. Cao, J. C. Shu, Y. Z. Cai, X. X. Wang, Q. L. Zhao and J. Yuan, *ACS Appl. Mater. Interfaces*, 2019, **11**, 12535–12543.

173 P. He, M. S. Cao, Y. Z. Cai, J. C. Shu, W. Q. Cao and J. Yuan, *Carbon*, 2020, **157**, 80–89.

174 Y. Li, X. Zhou, J. Wang, Q. Deng, M. Li, S. Du, Y. H. Han, J. Lee and Q. Huang, *RSC Adv.*, 2017, **7**, 24698–24708.

175 X. Li, W. You, C. Xu, L. Wang, L. Yang, Y. Li and R. Che, *Nano-Micro Lett.*, 2021, **13**, 157.

176 H. Zhao, Y. Cheng, H. Lv, G. Ji and Y. Du, *Carbon*, 2019, **142**, 245–253.

177 J. Cheng, C. Li, Y. Xiong, H. Zhang, H. Raza, S. Ullah, J. Wu, G. Zheng, Q. Cao, D. Zhang, Q. Zheng and R. Che, *Nano-Micro Lett.*, 2022, **14**, 80.

178 W. Zhang, X. Zhang, H. Wu, H. Yan and S. Qi, *J. Alloys Compd.*, 2018, **751**, 34–42.

179 Z. Xiang, Y. Shi, X. Zhu, L. Cai and W. Lu, *Nano-Micro Lett.*, 2021, **13**, 77–97.

180 P. He, M. S. Cao, W. Q. Cao and J. Yuan, *Nano-Micro Lett.*, 2021, **13**, 115.

181 L. C. Jia, D. X. Yan, C. H. Cui, X. Jiang, X. Ji and Z. M. Li, *J. Mater. Chem. C*, 2015, **3**, 9369–9378.

182 X. Cheng, X. Zhou, S. Wang, Z. Liu, Q. Liu, Y. Zhang, Q. Liu and B. Li, *Nanoscale Res. Lett.*, 2019, **14**, 1–9.

183 J. Carbonell, A. Díaz-Rubio, D. Torrent, F. Cervera, M. Kirleis, A. Piqué and J. Sánchez-Dehesa, *Sci. Rep.*, 2012, **2**, 558.

184 X. Wang, B. Zhang, W. Zhang, M. Yu, L. Cui, X. Cao and J. Liu, *Sci. Rep.*, 2017, **7**, 1584.

185 B. Deng, Z. Liu, F. Pan, Z. Xiang, X. Zhang and W. Lu, *J. Mater. Chem. A*, 2021, **9**, 3500–3510.

186 B. Ji, S. Fan, S. Kou, X. Xia, J. Deng, L. Cheng and L. Zhang, *Carbon*, 2021, **181**, 130–142.

187 S. Magdi, F. El-Diwany and M. A. Swillam, *Sci. Rep.*, 2019, **9**, 5829.

188 Y. Xing, Y. Wan, Z. Wu, J. Wang, S. Jiao and L. Liu, *ACS Appl. Mater. Interfaces*, 2023, **15**, 5787–5797.

189 Q. Zhang, J. Cui, S. Zhao, G. Zhang, A. Gao and Y. Yan, *Nanomaterials*, 2023, **13**, 417.

190 Y. Zhang, J. Kong and J. Gu, *Sci. Bull.*, 2022, **67**, 1413–1415.